Journal of Statistical Physics, Vol. 128, No. 4, August 2007 (© 2007)
DOI: 10.1007/s10955-007-9316-y

An Explicit Family of Probability Measures for Passive Scalar Diffusion in a Random Flow

Jared C. Bronski,[1] Roberto Camassa,[2] Zhi Lin,[2] Richard M. McLaughlin,[2,4] and Alberto Scotti[3]

Received November 23, 2005; accepted April 12, 2007
Published Online: June 27, 2007

We explore the evolution of the probability density function (PDF) for an initially deterministic passive scalar diffusing in the presence of a uni-directional, white-noise Gaussian velocity field. For a spatially Gaussian initial profile, we derive an exact spatio-temporal PDF for the scalar field renormalized by its spatial maximum. We use this problem as a test-bed for validating a numerical reconstruction procedure for the PDF via an inverse Laplace transform and orthogonal polynomial expansion. With the full PDF for a single Gaussian initial profile available, the orthogonal polynomial reconstruction procedure is carefully benchmarked, with special attentions to the singularities and the convergence criteria developed from the asymptotic study of the expansion coefficients, to motivate the use of different expansion schemes. Lastly, Monte-Carlo simulations stringently tested by the exact formulas for PDF's and moments offer complete pictures of the spatio-temporal evolution of the scalar PDF's for different initial data. Through these analyses, we identify how the random advection smooths the scalar PDF from an initial Dirac mass, to a measure with algebraic singularities at the extrema. Furthermore, the Péclet number is shown to be decisive in establishing the transition in the singularity structure of the PDF, from only one algebraic singularity at unit scalar values (small Péclet), to two algebraic singularities at both unit and zero scalar values (large Péclet).

KEY WORDS: Turbulent transport, probability measures, orthogonal polynomials, Monte-Carlo simulations

[1] Department of Mathematics, University of Illinois, Urbana, IL 61801, USA
[2] Department of Mathematics, University of North Carolina, Chapel Hill, NC 27599, USA
[3] Department of Marine Sciences, University of North Carolina, Chapel Hill, NC 27599, USA
[4] CB#3250, Phillips Hall, University of North Carolina, Chapel Hill, NC 27599-3250; e-mail: rmm@amath.unc.edu

1. INTRODUCTION

An extremely important and difficult class of statistical physics problems concerns the evolution of partial differential equations (PDE) with random coefficients. Physical examples include the behavior of Schrödinger equations with random potentials, light waves propagating in random media, and tracers advected by turbulent fluid flows. Partial differential equations are themselves generally viewed as infinite dimensional systems in finite dimensional spaces, and random PDE must somehow be understood as such systems. The example of turbulent convection has elucidated this point succinctly in a broad class of problems involving diffusing passive tracers in the presence of prescribed, random Gaussian random fluid flows[3,7,8,10,14,16,19,23,25] through the recognition that closed evolutions of the statistical moments are available in high-dimensional spaces. Experimental and observational data for tracer advections have demonstrated that effects of random advection may be responsible for setting a strongly non-Gaussian, heavy-tailed probability distribution function (PDF) for tracer fluctuations as observed both in controlled thermal convection experiments,[9,28] atmospheric wind measurements,[2] as well as observations of stratospheric inert tracers.[26]

The Chicago convection experiments[9] in fact motivated an enormous theoretical effort to understand this scalar intermittency (heavy-tailed scalar distributions) in the context of the linear evolution of a passive scalar diffusing in the presence of random advection, for extensive summary, see the review article by Majda and Kramer.[17] The general picture which has emerged is that rare, long lived, infinitesimal fluctuations in a random velocity are responsible for establishing the heavy tail in diffusing passive scalars. This picture is borne out through exact calculations involving the high moment asymptotics for statistical moments of the scalar fields,[8,16] through stochastic analysis,[29] through instanton type field theoretic calculations,[10] and through numerical simulation.[13,20] All of the theoretical calculations have involved highly idealized random flow geometries (either shear layers, or Batchelor flows). Even in those simplified geometries, only asymptotic information about the PDF tail is available.

To understand what is involved with calculating the PDF or the solution of a stochastic PDE, path integrals are generally unavoidable. To see this, consider the evolution of a diffusing passive tracer advected by a general stochastic velocity field $V_\omega(\vec{x}, t)$. Given a fixed realization of $V_\omega(\vec{x}, t)$, the scalar T is uniquely determined by the *Feynman-Kac's formula*:

$$T(\vec{x}, t) = E_{\mathbf{B}}[T_0(\vec{X}_{\mathbf{B},\omega}(t))] \tag{1.1}$$

where $E_{\mathbf{B}}$ is the statistical average over all the paths $\vec{X}_{\mathbf{B},\omega}(s)$, $0 \le s \le t$ which satisfies the *Stochastic Differential Equation*:

$$d\vec{X}_{\mathbf{B},\omega}(s) = -V_\omega(\vec{X}_{\mathbf{B},\omega}(s), t-s)\, ds + \sqrt{2\kappa}\, d\mathbf{B}(t), \qquad \vec{X}_{\mathbf{B},\omega}(0) = \vec{x} \tag{1.2}$$

with $\mathbf{B}(t)$ as the standard Brownian Motion and κ is the molecular diffusivity of the scalar. Therefore, the PDF for the scalar T conditioned on V_ω is a Dirac measure $\delta(T - E_{\mathbf{B}}[T_0(\vec{X}_{\mathbf{B},\omega}(t))])$. However, the unconditioned PDF for T is simply not tractable in general, since one has to integrate over all realizations of V_ω, namely,

$$P(T) = \int_\Omega p(T|V_\omega)p(V_\omega)\,d\mu(V_\omega) = \int_\Omega \delta(T - E_{\mathbf{B}}[T_0(\vec{X}_{\mathbf{B},\omega}(t))])p(V_\omega)\,d\mu(V_\omega) \tag{1.3}$$

where Ω is the space of all realizations of the random velocity field V_ω and $d\mu(V_\omega)$ is the measure associated to the particular path. When the velocity field admits randomness in both space and time, only very few analyses exist. For example, Kraichnan derived closed evolution equations for statistical moments in rapidly fluctuating fluid flows (white noise limit),[14] and Majda rigorously established, using path integral methods, the general evolution equation governing the N-point correlation function for stationary (in space and time) random shear layers.[15] Also, for scalar fields evolving in an imposed mean scalar gradient (a maintained, large-scale spatially linear scalar profile), Bourlioux and Majda have presented the long time PDF analysis for shear layers with a transverse, temporally varying wind field.[6] For some special cases in which the fluid flows are functionally dependent upon a finite number of stochastic processes $w_j(t)$,[3,7,8,10,16,19] progress can be made. For example, for fluid flows admitting a linear spatial structure (such as the Majda model which is a linear shear multiplied by temporally varying, Gaussian white noise), an explicit solution to the conditional Feynman-Kac solution in (1.1) is available by the method of characteristics. Even with this explicit, random Green's function, obtaining the complete probability measure for the random, advected scalar is not possible in general, and requires consideration of the second functional integral in (1.3). Currently, for random, spatially linear fluid flow, existing general results have succeeded in calculating, in closed form, the statistical moments and the PDF tail,[3,7,8,16,19,29] but not the full measure.

Our purpose here is to present a model for which the entire spatio-temporal PDF may be explicitly calculated, and use this model to develop numerical techniques which can be used to calculate a PDF from its statistical moments. By focusing on a uni-directional, constant in space, rapidly fluctuating (white in time), Gaussian random advection, we establish here a family of models for which the statistical moments are explicit simple algebraic expressions for any moment number, and for which the complete, explicit, spatio-temporal probability density function is available for specialized initial data. In turn, for more complex initial data, we present a reconstruction procedure based upon orthogonal polynomial expansion, which can approximate the exact PDF very well with a relative error of less than 1% when the first 4 moments are used for the summation, along

with high moment number moments asymptotically equal to true moments. Then we use these tools to benchmark Monte-Carlo simulations showing the spatio-temporal evolution of more general PDFs. These calculations give a rigorous and complete demonstration of the role which the Péclet number, a nondimensional number which measures the relative importance of advection versus diffusion, plays in adjusting the spatial structure of the PDF. Surprisingly, even in this simple flow, the interaction of advection with diffusion is very complicated, and the dynamics smooth in a precise way the initially Dirac scalar distributions for the deterministic initial data. The Péclet number is shown to move these algebraic singularities from the diffusion dominated regime, with probability focused at the highest scalar values, to the advective dominated regime, with probability collecting at the zero scalar value. For general models where only moment information is available, such as the Majda model,[7,8,16,19] the reconstruction procedure is also applicable, provided that the scalar can be renormalized onto a bounded interval, which will be explored in future work.

The paper is organized as follows: In Sec. 2, the simple, random advection-diffusion problem is mathematically formulated and the main results of this paper are presented. In Sec. 3, the formulas for the exact PDF and the statistical moments of the renormalized scalar field are derived, and we investigate some asymptotic limits of the PDF. Sections 4 and 5 present the theoretical analysis and numerical results of reconstructing the PDF from its statistical moments using orthogonal polynomials. Further, we show how modified regularization function and orthogonal basis improve the reconstruction, as well as the rigorous estimates of the decay rate of the Chebyshev coefficients in the series expansion. In Sec. 6, a Monte-Carlo simulator for the subject problem is developed and benchmarked for different initial data, whose results are used to study the spatio-temporal dynamics of the PDF of the scalar field. Lastly, the concluding remarks and some discussion on the future work are given in Sec. 7. The details of some calculations in the paper are listed in Appendix.

2. PROBLEM FORMULATION AND MAIN RESULTS

We consider the evolution of a decaying passive scalar with a random unidirectional, spatially constant wind, for ease in exposition, restricted to one spatial dimension. The governing stochastic PDE with Stratonovich's interpretation[12] is:

$$\begin{aligned} \frac{\partial T}{\partial t} + \gamma(t)\frac{\partial T}{\partial x} &= \kappa \frac{\partial^2 T}{\partial x^2}, \qquad -\infty < x < \infty, \quad t > 0 \\ T|_{t=0} &= T_0(x) \end{aligned} \tag{2.1}$$

where κ is the tracer's molecular diffusivity and $\gamma(t)$ is a Gaussian white noise, i.e.,

$$\langle \gamma(t) \rangle_\gamma = 0, \qquad \langle \gamma(t)\gamma(t') \rangle_\gamma = \sigma^2 \delta(t - t') \tag{2.2}$$

where $\langle \cdot \rangle_\gamma$ denotes the ensemble average over the statistics of γ.

Suppose that the initial data $T_0(x)$ has a typical length scale L. Then we have three dimensional parameters, σ^2, κ and L, from which we can only form one non-dimensional parameter for Eq. (2.1), the Péclet number $\mathrm{Pe} = \sigma^2/\kappa$, that characterizes the intensity of the random advection relative to molecular diffusion. If we let $x' = x/L$, $\tau = t\sigma^2/L^2$ and $\gamma'(\tau) = \gamma(t)L/\sigma^2$, the evolution of the tracer is governed by the non-dimensionalized equation

$$\begin{aligned} \frac{\partial T}{\partial \tau} + \gamma'(\tau)\frac{\partial T}{\partial x'} &= \frac{1}{\mathrm{Pe}}\,\frac{\partial^2 T}{\partial x'^2} \\ T|_{\tau=0} &= T_0'(x') \end{aligned} \tag{2.3}$$

where $\gamma'(\tau)$ is the non-dimensionalized white noise and $\langle \gamma'(\tau)\gamma'(\tau') \rangle_{\gamma'} = \delta(\tau - \tau')$. Notice that the length scale L does not appear in the Eq. (2.3). The initial length scale is irrelevant here since if we have a different length scale $\tilde{L}$ in the data, then letting $\tilde{x} = x'\tilde{L}/L$ and $\tilde{\tau} = \tau\tilde{L}^2/L^2$ will recover exactly the same Eq. (2.3) but in the variables $(\tilde{x}, \tilde{\tau})$. This feature is essentially introduced by the vanishing autocorrelation time of the white noise.

This particular time varying fluid flow, while trivial in spatial structure, gives rise to an interesting family of scalar probability measures. These measures give a connection between the respective limits of high and low Péclet number. At zero Péclet (no advection), the solution is trivial, and the ensuing probability measure for the values of the scalar field normalized by the spatial maximum is simply a Dirac mass (delta function) with support set by heat solution (see Result 1, and weak convergence calculations below in Sec. 2.5). At the alternative limit, we will see that in the limit of vanishing diffusion the probability measure for renormalized tracer values is also a Dirac mass (delta function) at large times, only with different support set. For finite, non-zero Péclet numbers, the probability measure is a smoother distribution, set by a competition between random advection and diffusion, which we can explicitly compute in this special case to see the connection between these two distributional limits.

The main results of this paper are the following:

Result 1. *For initial data $T_0(x) = e^{-x^2}$, at any fixed location x and time t, the random scalar $T(x,t)$ can be renormalized by a deterministic function $T_{\max}(t) = \frac{1}{\sqrt{4\kappa t+1}}$, so that the ensuing* probability density function *(PDF) for $\xi \equiv \frac{T(x,t)}{T_{\max}(t)}$ has*

compact support, namely,

$$\text{Prob}(\xi \notin [0,1]) = 0 \tag{2.4}$$

Moreover,

1. *The exact spatio-temporal PDF of the renormalized random scalar ξ is*

$$P_{x,t}(\xi) = \sqrt{\frac{1}{\beta\pi}}\ \frac{e^{-\frac{x^2}{a}}\ \xi^{\frac{1}{\beta}-1}\ \cosh\sqrt{-\frac{4b'x^2}{a^2}\ln\xi}}{\sqrt{-\ln\xi}} \tag{2.5}$$

for any $\xi \in (0,1)$, where

$$a = 2\sigma^2 t, \qquad b' = 4\kappa t + 1, \qquad \beta = a/b' \to \frac{\text{Pe}}{2}\ (t \to \infty) \tag{2.6}$$

This measure has a singular structure at $\xi = 1$ and if $\beta > 1, x \neq 0$, it is also singular at $\xi = 0$. It converges weakly to the Dirac delta measure $\delta(\xi)$ when $\beta \to \infty$ (high Péclet number limit for pure random advection) and to $\delta(\xi - e^{-\frac{x^2}{b'}})$ when $\beta \to 0$ (low Péclet number limit for pure diffusion).

2. *The Nth statistical moment of the random tracer $T(x,t)$ can be computed analytically as:*

$$\langle T^N(x,t)\rangle_\gamma = \frac{e^{-\frac{Nx^2}{Na+b'}}}{\sqrt{Nab'^{N-1}+b'^N}} \tag{2.7}$$

for $N = 0, 1, 2, \ldots$

3. *We formally expand the PDF of the renormalized random tracer by orthogonal polynomials as*

$$P_{x,t}(\xi) = \frac{\sum_{n=0}^{\infty} C_n\ Q_n(\xi)}{r(\xi)} \tag{2.8}$$

where $\{Q_n(\xi)\}_{n=0}^{\infty}$ is a family of orthogonal polynomials defined on $[-1,1]$ or $[0,1]$, $r(\xi)$ is a regularization function and the coefficients C_n are obtained from the statistical moments of the tracer (2.7). For a specific choice of the polynomial family and $r(\xi)$, the pointwise convergence of these reconstructions depends on the values of x and β. Given the convergence, the fact that $P(\xi)$ is compactly supported by $[0,1]$ guarantees the uniqueness of the expansion. Moreover, with the shifted Chebyshev polynomials, the reconstructed PDF has a relative error of less than 1% when the first 4 moments are used for the summation (2.8).

Result 2. *For the bimodal initial data $T_0(x) = \frac{\partial(e^{-x^2})}{\partial x} = 2xe^{-x^2}$, $T(x,t)$ can also be renormalized by $T_{\max}(t) = \frac{\sqrt{2e^{-1}}}{4\kappa t+1}$, such that* $\text{Prob}(\xi \notin [-1,1]) = 0$. *So again*

the probability measure is compactly supported. In this case, the exact, closed-form PDF for the renormalized tracer is available only in a long time limit and it is related to the two branches of the Lambert W-functions.[11] *However, the exact statistical moments of the random tracer $T(x,t)$ are still available at all times in analogy to (2.7). Thus we are able to reconstruct the PDF with orthogonal polynomials as described in Result 1.2.*

Result 3. *Monte-Carlo (MC) simulations, benchmarked on Result 1, present a detailed picture for the spatio-temporal evolution of the PDF when the exact solution to the moment problem is unknown. The simulation results also illustrate how different values of Péclet number change the spatial structure of the PDF. Further, simulations are preformed for initial data $T_0(x) = 2xe^{-x^2}$ and $T_0(x) = e^{-(x-A)^2} + e^{-(x+A)^2}$ respectively, for which exact PDF's at all times are not available.*

3. DERIVATION OF THE EXACT PDF AND MOMENTS

3.1. Exact PDF for $T_0(x) = e^{-x^2}$

For the unimodal, Gaussian initial data $T_0(x) = e^{-x^2}$, the exact PDF for the evolving random scalar field $T(x,t)$ can be computed analytically via direct statistical inversion, since

$$T(x,t) = \frac{1}{\sqrt{1+4\kappa t}} \exp\left(-\frac{(x-W(t))^2}{1+4\kappa t}\right) \tag{3.1.1}$$

which is a random translation of the pure heat solution, where $W(t) = \int_0^t \gamma(s)ds$ is a *Wiener Process*.[12] For example, when $x = 0$

$$\begin{aligned}\text{Prob}(\sqrt{1+4\kappa t}\ T(0,t) \le \xi) &= \text{Prob}\left(e^{-\frac{(W(t))^2}{1+4\kappa t}} \le \xi\right) \\ &= 1 - \text{Erf}\left(\sqrt{-\frac{1+4\kappa t}{2\sigma^2 t}\ \ln\xi}\right)\end{aligned} \tag{3.1.2}$$

where $\text{Erf}(\cdot)$ is the error function. Therefore, the ensuing probability density function is

$$P_{0,t}(\xi) := \frac{\partial}{\partial\xi}\left[1 - \text{Erf}\left(\sqrt{-\frac{1+4\kappa t}{2\sigma^2 t}\ \ln\xi}\right)\right] = \frac{\xi^{\frac{1}{\beta}-1}}{\sqrt{-\beta\pi\ln\xi}}. \tag{3.1.3}$$

with $\beta = \frac{2\sigma^2 t}{1+4\kappa t}$. To recover the general case (2.5) for $x \neq 0$, similar but more complicated algebra as in Eq. (3.1.2) is needed. Instead, we follow an alternative derivation using Laplace inversion in Sec. 3.4.

3.2. Exact Statistical Moments for General Initial Data

For general initial data, the direct statistical inversion technique shown in Eq. (3.1.2) is not always applicable, even when an analytic solution similar to Eq. (3.1.1) is available. However, the exact statistical moments of the random scalar are often accessible. The solution to Eq. (2.1) can be written via Fourier transform as:

$$T(x,t) = \int_{-\infty}^{\infty} e^{2\pi i k[x - W(t)] - 4\pi^2 \kappa k^2 t}\ \hat{T}_0(k)\, dk \tag{3.2.1}$$

where $\hat{T}_0(k)$ is the Fourier transform of $T_0(x)$. In fact, this is just a "drifted" version of the fundamental heat solution, spatially shifted by $-W(t)$. Consequently, we have the following formula for arbitrary moments of the tracer field, T, satisfying Eq. (2.1):

$$\langle T^N(x,t)\rangle_\gamma = \left\langle \prod_{j=1}^{N} T(x_j,t) \right\rangle_\gamma = \int_{R^N} e^{2\pi i \mathbf{k}\cdot\mathbf{x} - 4\pi^2\kappa|\mathbf{k}|^2 t} \left\langle e^{-2\pi i \sum_{j=1}^{N} k_j W(t)} \right\rangle_\gamma \prod_{j=1}^{N} \hat{T}_0(k_j)\, d\mathbf{k} \tag{3.2.2}$$

with $\mathbf{x} = (x_1, x_2, \ldots, x_N) = (x, x, \ldots, x)$ and $\mathbf{k} = (k_1, k_2, \ldots, k_N)$.

Since $-2\pi i \sum_{j=1}^{N} k_j\ W(t)$ is a mean-zero, Gaussian random variable, we have

$$\left\langle e^{-2\pi i \sum_{j=1}^{N} k_j\ W(t)} \right\rangle_\gamma = e^{-2\pi^2\sigma^2 t (\sum_{j=1}^{N} k_j)^2}. \tag{3.2.3}$$

and Eq. (3.2.2) reduces to

$$\langle T^N \rangle_\gamma = \int_{R^N} e^{2\pi i \mathbf{k}\cdot\mathbf{x} - \mathbf{k}^T A_N \mathbf{k}} \prod_{j=1}^{N} \hat{T}_0(k_j)\, d\mathbf{k} \tag{3.2.4}$$

where

$$A_N = \pi^2 \begin{pmatrix} a+b & a & \cdots & a \\ a & a+b & \cdots & a \\ \cdots & \cdots & \cdots & \cdots \\ a & a & \cdots & a+b \end{pmatrix} \tag{3.2.5}$$

with

$$a = 2\sigma^2 t \qquad \text{and} \qquad b = 4\kappa t \tag{3.2.6}$$

Since A_N is *symmetric positive definite*, computing the exact moments is equivalent to diagonalizing a quadratic form. We start with the special case

$$T_0(x) = \delta(x) \tag{3.2.7}$$

and thus $\prod_{j=1}^{N} \hat{T}_0(k_j) = 1$. The familiar result for a N-dimensional Gaussian integral reads:

$$\langle T^N(0,t)\rangle = \int_{R^N} e^{-\mathbf{k}^T A_N \mathbf{k}} d\mathbf{k} = \frac{\pi^{\frac{N}{2}}}{\sqrt{\det A_N}} \tag{3.2.8}$$

The determinant in the denominator does not vanish provided $b \neq 0$ in Eq. (3.2.6) and it can be easily shown by induction that $\det A_N = \pi^{2N}(Nab^{N-1} + b^N)$. For $x \neq 0$, we need to diagonalize A_N as $A_N = V'\Lambda V$ where $V = \{\vec{v}_i\}_{i=1}^N = \{v_{ij}\}_{i,j=1}^N$ is the orthogonal matrix composed of A_N's eigenvectors and Λ is the diagonal matrix of its eigenvalues. Changing variables by $\bar{\mathbf{k}} = V\mathbf{k}$, Eq. (3.2.4) becomes:

$$\begin{aligned}
\langle T^N(x,t)\rangle_\gamma &= \int_{R^N} e^{2\pi i x \sum_{m,n=1}^{N} \bar{k}_m v_{mn} - \pi^2 b \sum_{m=1}^{N-1} \bar{k}_m^2 - \pi^2 (Na+b)\bar{k}_N^2} d\bar{\mathbf{k}} \\
&= \frac{\pi^{\frac{N}{2}}}{\sqrt{\det A_N}}\, e^{-x^2\left(\frac{\sum_{m=1}^{N-1} v_m^2}{b} + \frac{v_N^2}{Na+b}\right)} \\
&= \frac{\pi^{-\frac{N}{2}}}{\sqrt{Nab^{N-1} + b^N}}\, e^{-\frac{Nx^2}{Na+b}}
\end{aligned} \tag{3.2.9}$$

where $V_m = \sum_{n=1}^{N} v_{mn}$, $m = 1, 2, \ldots, N$. We will prove Eq. (3.2.9) by showing $V_m = 0$ for $m < N$, $V_N = \sqrt{N}$ in Appendix. In particular, when $x = 0$, we retrieve formula (3.2.8).

To generalize Eq. (3.2.9) for arbitrary $T_0(x)$, we just apply the Convolution Theorem to Eq. (3.2.2) and read

$$\langle T^N\rangle_\gamma = \frac{\pi^{\frac{N}{2}}}{\sqrt{\det A_N}} \int_{\mathbb{R}^N} \exp\left(-\frac{1}{b}\left[|\mathbf{y}|^2 - \frac{a\left(\sum_{j=1}^{N} y_j\right)^2}{aN+b}\right]\right) \prod_{j=1}^{N} T_0(x - y_j)\, d\mathbf{y} \tag{3.2.10}$$

In particular, for $T_0(x) = e^{-x^2}$, Eq. (2.7) is recovered by computing the above integral, which is the same as in the case of $T_0(x) = \delta(x)$ except that b is replaced by $b' = b + 1$.

Now we introduce the random variable $\xi := \frac{T(x,t)}{T_{\max}(t)}$ and its Nth-order statistical moment $M_N := \langle \xi^N \rangle_\gamma$ and we denote its PDF by $P_{x,t}(\xi)$. Since

$$M_N = \int_{-\infty}^{\infty} \xi^N P_{x,t}(\xi)\, d\xi \geq \int_1^{\infty} \xi^N P_{x,t}(\xi)\, d\xi \geq \int_1^{\infty} P_{x,t}(\xi)\, d\xi = \text{Prob}(\xi > 1) \tag{3.2.11}$$

and from Eq. (2.7)

$$M_N = \frac{\langle T^N(x,t)\rangle_\gamma}{T^N_{\max}(t)} = \frac{e^{-\frac{Nx^2}{aN+b'}}}{\sqrt{1+\beta N}} \to 0 \tag{3.2.12}$$

as $N \to \infty$, we conclude that $\text{Prob}(\xi > 1) = 0$ which ultimately leads to Eq. (2.4). This seems redundant here by the simple definition of ξ, while an analogous argument is useful to infer a compactly-supported measure when only the moment information of ξ is available.

3.3. Long Time Asymptotics of the Moments

In the long-time limit, we can apply Eq. (3.2.8) to study the asymptotic behavior of the moments for more general initial conditions and at locations away from the origin. Without loss of generality, we use some of the results from Eq. (3.2.9) through (3.2.10) and consider

$$\langle T^N\rangle_\gamma = \int_{-\infty}^{\infty} e^{2\pi i\sqrt{N}x\bar{k}_N - \pi^2(Na+b)\bar{k}_N^2 - \pi^2 b\sum_{n=1}^{N-1}\bar{k}_n^2} \prod_{n=1}^{N} \hat{T}_0(\bar{k}_n)\, d\bar{\mathbf{k}} \tag{3.3.1}$$

for an unknown, general $T_0(x)$. For a large time t, if we rescale $\bar{\mathbf{k}}$ as $\bar{\mathbf{k}} = \frac{\mathbf{k}}{\sqrt{t}}$, when $t \to \infty$,

$$\begin{aligned}
\langle T^N\rangle_\gamma &= \int_{-\infty}^{\infty} e^{2\pi i\sqrt{N}x\bar{k}_N - \pi^2(Na+b)\bar{k}_N^2 - \pi^2 b\sum_{n=1}^{N-1}\bar{k}_n^2} \prod_{n=1}^{N} \hat{T}_0(\bar{k}_n)\, d\bar{\mathbf{k}} \\
&= t^{-\frac{N}{2}} \int_{-\infty}^{\infty} e^{2\pi i\sqrt{N}x\frac{k_N}{\sqrt{t}} - \pi^2\frac{Na+b}{t}k_N^2 - \pi^2\frac{b}{t}\sum_{n=1}^{N-1}k_n^2} \prod_{n=1}^{N} \hat{T}_0\left(\frac{k_n}{\sqrt{t}}\right) d\mathbf{k} \qquad (3.3.2) \\
&\sim \left(\frac{\pi\hat{T}_0^2(0)}{4\kappa t}\right)^{\frac{N}{2}} \frac{1}{\sqrt{1+\sigma^2 N/(2\kappa)}}
\end{aligned}$$

provided $\hat{T}_0(0) \neq 0$ and the quantities $\frac{a}{t}$ and $\frac{b}{t}$ have finite limits as $t \to \infty$, which is guaranteed by definition (3.2.6) given finite σ^2 and κ. Therefore, in the long time limit, the statistical moments of T are independent of x. To see this, observe that the last two factors in the exponent of the exponential are time-independent constants through Eq. (3.2.6). Consequently the complex part of the exponential is subdominant at long time. Notice that this asymptotic convergence should be uniform only over compact sets, which will be illustrated in Section 6 without a rigorous proof. More importantly, from Eq. (3.3.2), the tracer field can be renormalized such that the moments of the renormalized tracer ξ, $\langle \xi^N\rangle$, are asymptotically *self-similar*, namely, independent of *both* x and t for large times.

3.4. Exact PDF and the Inverse Laplace Transform of the Moment Function

The problem of determining a compactly-supported measure $P(\xi)\,d\xi$ from its moments is known as the *Hausdorff Moment Problem*. Once the exact moment of arbitrary order is determined, the problem has a unique solution.[24] Define the *moment function* of $P(\xi)$ as

$$\mu(s) = \int_0^1 \xi^s P(\xi)\,d\xi = \int_0^\infty e^{-st} e^{-t} P(e^{-t})\,dt = \mathcal{L}[e^{-t}P(e^{-t})](s) \qquad (3.4.1)$$

whose values evaluated at $s = 0, 1, 2, \ldots$ are exactly the statistical moments of P. Then

$$P(\xi) = \frac{\mathcal{L}^{-1}[\mu(s)](-\ln\xi)}{\xi} \qquad (3.4.2)$$

For the particular initial data $T_0(x) = e^{-x^2}$, we know from Eq. (2.4) that the PDF of the renormalized tracer ξ is compactly supported by $[0, 1]$. Now define

$$\mu^*(s) := \frac{e^{-\frac{sx^2}{as+b'}}}{\sqrt{1+\beta s}}. \qquad (3.4.3)$$

It follows from Eq. (3.2.12) that $\mu^*(N) = \langle \xi^N \rangle_\gamma$ for $N = 0, 1, 2, \ldots$. If $\mu(t) \equiv \mu^*(t)$, the exact PDF (2.5) for the renormalized random tracer can also be derived via the inverse Laplace Transform of $\mu^*(t)$ through Eq. (3.4.2). The necessary and sufficient conditions for $\mu(t) \equiv \mu^*(t)$ may be found in the literature.[24] However, these conditions appear difficult to verify analytically. Alternatively, we perform the Laplace Transform for $\mu^*(t)$ and compare *a posteriori* the result with Eq. (2.5). First notice that

$$\mu^*(s) = \frac{\sqrt{a}}{x}\, e^{-\frac{x^2}{a}} \frac{e^{\frac{1}{s'}}}{\sqrt{s'}} = \frac{\sqrt{a}}{x}\, e^{-\frac{x^2}{a}} \bar{\mu}(s') \qquad (3.4.4)$$

with $s' = \frac{a^2 s}{x^2 b'} + \frac{a}{x^2}$ and we assume $a, b', x \neq 0$ without loss of generality. We can show that[1]

$$\begin{aligned} \mathcal{L}^{-1}[\mu^*(s)](t) &= \frac{\sqrt{a}}{x}\, e^{-\frac{x^2}{a}} \mathcal{L}^{-1}\left[\bar{\mu}\left(\frac{a^2 s}{x^2 b'} + \frac{a}{x^2}\right)\right](t) \\ &= \frac{b'\sqrt{a}}{a^2 x} e^{-\frac{x^2}{a} - \frac{b'}{a}t} \mathcal{L}^{-1}[\bar{\mu}(s)]\left(\frac{b' x^2 t}{a^2}\right) \\ &= \sqrt{\frac{1}{\beta\pi}}\, \frac{e^{-\frac{t}{\beta} - \frac{x^2}{a}}\, \cosh\sqrt{\frac{4b'x^2 t}{a^2}}}{\sqrt{t}}. \end{aligned} \qquad (3.4.5)$$

Assuming $\mu(t) \equiv \mu^*(t)$, then Eq. (3.4.2) and Eq. (3.4.5) yield the explicit formula for $P_{x,t}(\xi)$ which is identical to Eq. (2.5).

3.5. Distinguished Limits of the Péclet Number for $T_0(x) = e^{-x^2}$

If we consider the special case $x = 0$ for the exact moments Eq. (3.2.12) for the renormalized tracer ξ, two special cases emerge:

1. $0 < \beta \ll 1$. In the limit $\beta \to 0$ evidently $\langle \xi^N \rangle_\gamma \to 1$ for any N.
2. $\beta \gg 1$. In the limit $\beta \to \infty$ $\langle \xi^N \rangle_\gamma \to 0$ for any $N > 0$ except $N = 0$.

These two cases can be interpreted as the weak convergence of the PDF

$$P_{x,t}(\xi) = \sqrt{\frac{1}{\beta\pi}} \frac{\xi^{\frac{1}{\beta}-1}}{\sqrt{-\ln \xi}} \tag{3.5.1}$$

to Dirac delta measures when $\beta \to 0/\infty$. An important fact is that for fixed σ and κ, β is an increasing function of t and

$$\lim_{t\to\infty} \beta = \lim_{t\to\infty} \frac{2\sigma^2 t}{1 + 4\kappa t} = \frac{\sigma^2}{2\kappa} = \frac{\mathrm{Pe}}{2}. \tag{3.5.2}$$

It is not hard to generalize this result for $x \neq 0$ in the long time limit, from Eq. (3.3.3), since $P_{x,t}(\xi)$ is independent of x and it is only controlled by the Péclet number. Consequently, the distinguished limits of $P_{x,t}(\xi)$ at large times as $\mathrm{Pe} \to 0/\infty$ are equivalent to the singular limits as $\beta \to 0/\infty$. For any test function $\phi(\xi)$ defined on $[0, 1]$, we have

$$\begin{aligned} \int_0^1 P_{x,t}(\xi)\phi(\xi)\,d\xi &= \frac{1}{\sqrt{\pi}} \int_0^1 \sqrt{\frac{1}{\beta}} \frac{e^{-\frac{x^2}{a}} \xi^{\frac{1}{\beta}-1} \cosh\left(2\sqrt{-\frac{b'x^2}{a^2}\ln\xi}\right)\phi(\xi)}{\sqrt{-\ln\xi}}\,d\xi \\ &\approx \frac{2}{\sqrt{\pi}} \int_0^\infty e^{-y^2} \phi\left(e^{-(\sqrt{\beta}\,y - \frac{x}{\sqrt{b'}})^2}\right) dy \end{aligned} \tag{3.5.3}$$

after the change of variable $y = \sqrt{\frac{-\ln\xi}{\beta}} + \frac{x}{\sqrt{a}}$. Thus formally

$$\int_0^1 P_{0,t}(\xi)\phi(\xi)\,d\xi \to \begin{cases} \frac{2}{\sqrt{\pi}}\phi\left(e^{-\frac{x^2}{b'}}\right) \int_0^\infty e^{-y^2}\,dy = \phi(e^{-\frac{x^2}{b'}}), & \beta \to 0 \\ \frac{2}{\sqrt{\pi}}\phi(0) \int_0^\infty e^{-y^2}\,dy = \phi(0), & \beta \to \infty \end{cases} \tag{3.5.4}$$

Therefore $P_{x,t}(\xi)$ converges to $\delta(\xi - e^{-\frac{x^2}{\beta t}})$, which is exactly a Dirac delta measure at the pure heat solution, as $\beta \to 0$ and to $\delta(\xi)$ as $\beta \to \infty$, in a distributional sense. When β goes to 0, the random effects becomes negligible and the original Eq. (2.1) "degenerates" to a simple, deterministic heat equation. Thus the tracer will always be the pure heat solution with probability 1. In contrast, when $\beta \to \infty$, at any fixed spatial location x, the deterministic pure solution at that location is shifted by the random drift so far away, that $T(x, t)$ will almost certainly assume the infinitesimal values in the tails of the flattening Gaussian profile, namely, $T(x, t) = 0$ with probability 1.

For intermediate values of β, as we will see in the next section, the large moment asymptotics provide valuable information for the reconstruction of the PDF via orthogonal polynomials, when the exact PDF is unknown. Further, the values of β and x determine the convergence of the series reconstruction.

4. PDF RECONSTRUCTION FROM MOMENTS USING ORTHOGONAL POLYNOMIAL APPROXIMANTS

4.1. Motivation

As we mentioned before, the exact PDF for a tracer undergoing random advection and diffusion is generally unavailable while the exact moments are often accessible. Eq. (3.1.2) and (3.2.12) showed that renormalizing the moments of $T(x, t)$ by the maximum of the heat solution for $T_0(x) = e^{-x^2}$ leads to a measure compactly-supported by the interval [0, 1]. Techniques to reconstruct the *distribution function* $D(\xi) = \int_a^\xi P(s)ds$ via Legendre polynomials using the moments exist in literature,[24] when the density function $P(\xi)$ is compactly supported. However, the resulting distribution function will always be of bounded variations, while the PDF's we derived above have singularities and thus do not have a convergent, canonical Legendre expansion. Therefore in this paper, we seek for a direct polynomial reconstruction for the PDF, with coefficients also determined by the exact statistical moments. As a test problem, we implement this idea to the case $T_0(x) = e^{-x^2}$, for which the exact PDF (2.5) benchmarks the procedure and in turn we use the reconstructions to infer the behavior of more complicated measures.

4.2. Choice of Orthogonal Polynomials

To reconstruct the PDF as a series expansion, first we have to make a choice on the family of orthogonal polynomials defined on a bounded domain. Two canonical choices of such polynomials are Legendre polynomials and Chebyshev polynomials. We elect to use the Chebyshev polynomials of the first kind because, as we now show, the large moment asymptotics of our unknown PDF have the same scalings as those induced by any linear combination of orthonormal

Chebyshev polynomials. The key to verify this assertion lies in the particular weight function, $(\sqrt{1-\xi^2})^{-1}$, for Chebyshev polynomials. Observe that if the measure is approximated as the zeroth order Chebyshev polynomial divided by the weight function and multiplied by a normalization constant

$$P_{0,t}(\xi) \approx \frac{2\ T_0(\xi)}{\pi\sqrt{1-\xi^2}} = \frac{2}{\pi\sqrt{1-\xi^2}},$$

then the large moment asymptotics are given by the following sequence of calculations:

$$\frac{\pi}{2}\langle \xi^N \rangle_\gamma \approx \int_0^1 \frac{\xi^N}{\sqrt{1-\xi^2}} d\xi = \int_0^\infty \frac{e^{-(N+1)u}}{\sqrt{1-e^{-2u}}}\, du \sim \sqrt{\frac{\pi}{2}}\frac{1}{\sqrt{N+1}} \tag{4.2.1}$$

when N is large. This has the same large N asymptotic scalings as the moments given in Eq. (3.2.12) when $\beta = 1$ and $x = 0$. Moreover, it is natural to anticipate a singularity in the PDF at $\xi = 1$, introduced by $\sqrt{1-\xi^2}$ in the denominator, since the initial PDF at $x = 0$ is a Dirac delta function $\delta(\xi - 1)$.

We next assume that $P_{x,t}(\xi)$ has the following formal series representation:

$$P_{x,t}(\xi) = \frac{\sum_{m=0}^\infty C_m T_m(\xi)}{\sqrt{1-\xi^2}} \tag{4.2.2}$$

where $T_m(x)$, $m = 0, 1, \ldots$ is the mth order Chebyshev polynomial of the first kind. As we will next see, this ansatz will lead to great simplification for the construction of the PDF. Again, Eq. (4.2.2) assumes a singularity at $\xi = 1$. In fact, in the absence of random advection, $\beta = a/b' = 0$, $P_{0,t}$ is nothing more than a Dirac delta function $\delta(\xi - 1)$, which is singular at 1. As β increases, the random drift causes non-vanishing probability for $\xi \neq 1$. But when a is "not too big," it is reasonable to assume that the singularity at $\xi = 1$ persists. For $x \neq 0$, this is still physically plausible because of the diffusive property of the equation. Indeed, with the exact PDF known in this case, the singularity is obvious from Eq. (2.5).

4.3. Obtaining the Expansion Coefficients via Extensions of the PDF

The Chebyshev polynomials are defined on $[-1, 1]$ whereas $P_{x,t}$ is on $[0, 1]$. We may easily extend $P_{x,t}$, evenly or oddly, to $[-1, 1]$, to make use of standard Chebyshev identities. Denote the extended PDF as $\widetilde{P}_{x,t}$. The coefficients C_n may then be computed directly in terms of the moments, $M_n = \langle \xi^N \rangle_\gamma$, through the orthogonality of the Chebyshev polynomials, to wit:

$$\int_{-1}^1 T_n(\xi)\widetilde{P}_{x,t}(\xi) d\xi = \int_{-1}^1 \frac{\sum_{m=0}^\infty C_m T_m(\xi) T_n(\xi)}{\sqrt{1-\xi^2}}\, d\xi = C_n\ w_n \tag{4.3.1}$$

where w_n, the norm of $T_n(\xi)$ squared with weighting function $\frac{1}{\sqrt{1-\xi^2}}$, is π when $n = 0$ and $\frac{\pi}{2}$ otherwise; at the same time

$$\int_{-1}^{1} T_n(\xi)\widetilde{P}_{x,t}(\xi)d\xi = \int_{-1}^{1} \sum_{m=0}^{n} b_{nm}\xi^n \widetilde{P}_{x,t}(\xi)\, d\xi$$

$$= \sum_{m=0}^{n} b_{nm} \int_{-1}^{1} \xi^n \widetilde{P}_{x,t}(\xi)\, d\xi = \sum_{m=0}^{n} b_{nm}\widetilde{M}_m \quad (4.3.2)$$

where

- $B = \{b_{nm}\}_{n,m=0}^{\infty}$ is the transfer matrix from the monomial basis $\{\xi^n\}_{n=0}^{\infty}$ to the Chebyshev basis $\{T_n(\xi)\}_{n=0}^{\infty}$;
- $\widetilde{M}_m$ is the mth moments of $\widetilde{P}_{x,t}$, namely, for even extension $\widetilde{M}_n = 2M_n$ if n is even and $\widetilde{M}_n = 0$ otherwise, and *vice versa* for odd extension.

Therefore, equating the right-hand-sides of Eqs. (4.3.1) and (4.3.2), for even extension we have only the even-ordered terms survived in the series expansion (4.2.2), namely, $C_{2n-1} = 0,\ n = 1, 2, \ldots$. Plugging in explicit formulas for b_{nm} [(1)] and $\widetilde{M}_m$, we have $C_0 = \frac{2}{\pi}$ and

$$C_{2n} = \frac{\sum_{m=0}^{2n} b_{2n,m}\widetilde{M}_m}{w_{2n}} = \frac{(-1)^n n}{\pi} \sum_{m=0}^{n} \frac{(-1)^m\ 2^{2m+2}\ (n+m-1)!}{(n-m)!\ (2m)!} \frac{e^{-\frac{2mx^2}{2ma+b'}}}{\sqrt{1+2\beta m}} \quad (4.3.3)$$

for $n = 1, 2, \ldots$. Alternatively, we can invert the above formula to get

$$M_{2n} = \frac{4^{n-1}\Gamma^2(n)}{\pi\Gamma(2n)} \sum_{m=0}^{n} C_{2m}\ \bar{w}_{2m}, \quad n = 1, 2, \ldots \quad (4.3.4)$$

with $\bar{w}_m = 1$ if $m = 0$ and $\bar{w}_m = 2$ otherwise. This is a finite sum and it suggests that for any fixed $N > 0$, the $2N$-term truncation of the series (4.2.2) with coefficients $C_m, m = 0, 1, \ldots, 2N-1$ defined above will generate the first N even moments identical to those of the true PDF. Furthermore, utilizing (3.2.12) and the asymptotic property of Gamma functions,[(1)] if we define $C_{2N} = \sqrt{\pi/(2\beta)}e^{-\frac{x^2}{a}} - \sum_{m=1}^{N-1} C_{2m} - \frac{1}{2}C_0$, the resulting $(2N+1)$-term truncation will have large evenmoments M_{2n}^a asymptotically equal to the true moments

Table I. $P_{x,t}(0)$ for Different x's and β's

$P_{x,t}(0)$	$x = 0$	$x \neq 0$
$\beta < 1$	0	0
$\beta = 1$	0	∞
$\beta > 1$	∞	∞

M_{2n} as $n \to \infty$, since

$$M_{2n}^a = \frac{4^{n-1}\Gamma^2(n)}{\pi\Gamma(2n)} \sum_{m=0}^{N} C_{2m}\ \bar{w}_{2m}$$

$$= \frac{2^{2n-1}\Gamma^2(n)}{\Gamma(2n)\sqrt{2\pi\beta}}\, e^{-\frac{x^2}{a}} \sim \frac{e^{-\frac{x^2}{a}}}{\sqrt{2\beta n}} \sim M_{2n}, \quad n \to \infty. \tag{4.3.5}$$

It may seem unusual that we are able to reconstruct the measure using only half of the moments, namely, even or odd. However, this is justified through the *Müntz-Szasz Theorem*,[22] which guarantees us that the expansion of $P_{x,t}(\xi)$ using only the Chebyshev polynomials with even powers in Eq. (4.2.2) is unique and it assumes pointwise convergence on $[0, 1]$, if $\sqrt{1-\xi^2}P_{x,t}(\xi) \in \mathcal{C}[0, 1]$. Essentially, it is because the expansion can be re-written as a linear combination of $\{x^{\lambda_i}\}_{i=0}^{\infty}$, where $\lambda_i = 2i$ which satisfies $\sum_{i=0}^{\infty} \frac{1}{\lambda_i} = \infty$. Thus, these polynomials are dense in $\mathcal{C}[0, 1]$ and can be extended to $\mathcal{C}[-1, 1]$ without any complication. This is also true for the odd extension case, except that we have to assume $P_{x,t}(0) = 0$ such that $\sqrt{1-\xi^2}\ P_{x,t}(\xi)$ is continuous at $\xi = 0$ to apply the result. However, this assumption may be false for some values of x and β. Recall the exact PDF (2.5) and the fact $P_{x,t}(0) := \lim_{\xi \to 0^+} P_{x,t}(\xi)$, Table 1 summarizes the values of $P_{x,t}(0)$ for different x's and β's and whenever $P_{x,t}(0) = \infty$, the expansion is not convergent at $\xi = 0$, since in such cases $\sqrt{1-\xi^2}P_{x,t}(\xi) \notin \mathcal{C}[0, 1]$. This leads to the next discussion on the role $\sqrt{1-\xi^2}$ is playing.

4.4. Regularization Function

It is known that any continuous function on $[-1, 1]$ can be expanded as a pointwise convergent series with Chebyshev polynomials.[18] And from Eqs. (4.2.2) and (4.3.1), it is clear that we are essentially expanding the function $f(\xi) = \sqrt{1-\xi^2}P_{x,t}(\xi)$. However, Table 1 suggests that the series does not always converge pointwise, since $f(0)$ may diverge. This is not surprising from the exact formula of the PDF (2.5) because $f(\xi)$ can be discontinuous at $\xi = 0$ when $\beta > 1$ or $x \neq 0$. As we will see in the next section, this will lead to the

failure of the numerical series reconstruction, as the sum of polynomials diverges at the singularities.

Now we see that, if we can find a proper *regularization function* $r(\xi)$ such that $f(\xi) = r(\xi)\widetilde{P}_{x,t}(\xi)$ belongs to, or can be extended continuously to $\mathcal{C}[-1, 1]$, its series expansion will assume pointwise convergence in $[-1, 1]$, whose coefficients should still be computed from the statistical moments, namely,

$$\begin{aligned} f_n w_n &= \int_{-1}^{1} f\ Q_n\ w\ d\xi = \int_{-1}^{1} r\ \widetilde{P}\ Q_n\ w\ d\xi \\ &= \int_{-1}^{1} \xi^k\ \widetilde{P}\ Q_n\ d\xi = \sum_{m=0}^{n} b_{nm} \widetilde{M}_{m+k} \end{aligned} \tag{4.4.1}$$

in which k is a non-negative integer and f, Q_n, w, r and $\widetilde{P}$ are all functions of ξ. For example, in the previous discussion, $r(\xi)$ was taken to be $1/w(\xi) = \sqrt{1-\xi^2}$. Consequently, $k = 0$ in Eq. (4.4.1) and we recover the formula for $f_n = C_n$ shown in Eq. (4.3.2). It can be verified that this leads to $f(0) = \infty$; while for $r(\xi) = \xi\sqrt{1-\xi^2}$, $f(0) = 0$ for any x and β, yet it still allows us to compute the coefficients in the series using statistical moments by making $r(\xi)w(\xi) = \xi$ and thus $k = 1$ in Eq. (4.4.1).

Moreover, the extensions for the PDF can be avoided by using alternative families of orthogonal polynomials for different $r(\xi)$, then the interval $[-1, 1]$ can be replaced with $[0, 1]$. One of these families is the *shifted Chebyshev polynomials* of the first kind, $T_n^*(\xi) = T_{2n}(\sqrt{\xi})$, $n = 0, 1, 2, \ldots$ for any $\xi \in [0, 1]$, and the corresponding weight function is $w^*(\xi) = 1/\sqrt{\xi(1-\xi)}$. The motivation of choosing this family is to capture the singularity at $\xi = 0$, which is smoothed out by extension if standard Chebyshev polynomials are used. A similar calculation as in Eq. (4.2.1) shows that they also yield the same large n asymptotic scaling for the moments. Further, if we re-define $r(\xi) = \sqrt{\xi^3(1-\xi)}$, Eq. (4.4.1) is then modified as

$$\begin{aligned} f_n w_n &= \int_0^1 r(\xi)\ P(\xi)\ T_n^*(\xi)\ w^*(\xi)\ d\xi \\ &= \int_0^1 \xi\ P(\xi)\ Q_n(\xi)\ d\xi = \sum_{m=0}^{n} b_{nm} M_{m+1}. \end{aligned} \tag{4.4.2}$$

It is not hard to show that $f(\xi) = \sqrt{\xi^3(1-\xi)}\ P(\xi)$ for any probability measure P singular at 0 can be extended continuously to $\mathcal{C}[0, 1]$ and the series expansion converges pointwise for any x and β, from the integrability of P. Consequently the coefficients in the ansatz (2.8) with $Q_n(\xi) = T_n^*(\xi)$ is obtained by

similar calculations as in Eq. (4.3.1) through (4.3.3) which read

$$C_n w_n = \sum_{m=0}^{n} b_{nm} M_{m+1} \tag{4.4.3}$$

where again, M is the statistical moment, $\{b_{nm}\}_{n,m=0}^{\infty}$ is the transfer matrix and w_n is the normalization constant. Notice that $M_0 = 1$ is not present in the computation. In the next section, some examples show how this orthogonal basis improves the reconstruction.

Further, this idea can potentially be generalized to any PDF without *a priori* knowledge of its singular structure other than the locations of the singularities, since one can always choose the regularization function to be the product between the weight function of the orthogonal basis, $w(\xi)$, and $\prod_{i=1}^{N}(\xi - \xi_i^*)$, in which $\xi_i^*, i = 1, \ldots, N$ are the points where $P(s_i)$ diverges, to meet the requirements of 1) the convergence of the series expansion and 2) the computability of the coefficients from the moments. However, one does need to identify ξ_i^* before the expansion, either from physical or mathematical considerations, which we have mentioned in Sec. 4.2 and we will revisit this in Sec. 6.4. Notice that even if $P(\xi^*) < \infty$ for some ξ^*, it is clear that the series expansion still converges and we can still extract the correct PDF. Thus, we can remove all the possible singularities for series expansion to guarantee the convergence.

4.5. Large-n Asymptotics of the Coefficients C_n

Of course, the choice of polynomial family is not restricted to Chebyshev polynomials. For example, we can also re-define $r(\xi) = \xi(1 - \xi)$ and use Legendre polynomials for reconstruction. Nonetheless, a Chebyshev basis does allow us to have a rigorous estimate of the remainder of the series, by applying the *method of steepest descent* to study the asymptotic behavior of the coefficients C_n for n large. For $Q_n(\xi) = T_n(\xi)$, we can explicitly compute

$$C_{2n} = 2Re\left[\int_0^{\frac{\pi}{2}} e^{i2n\theta} \sin\theta \, \frac{e^{-\frac{x^2}{a}} (\cos\theta)^{\frac{1}{\beta}-1} \cosh\sqrt{-\frac{4b'x^2}{a^2}\ln(\cos\theta)}}{\sqrt{-\beta\pi \ln(\cos\theta)}} \, d\theta\right] \tag{4.5.1}$$

and $C_{2n+1} = 0$ for $n = 0, 1, 2, \ldots$, utilizing the fundamental property of Chebyshev polynomials, $T_n(\xi) = \cos(n\theta)$ where $\theta = \cos^{-1}(\xi)$. And the large n asymptotics of C_{2n} is revealed through evaluating the integral of the complex function

$$I(z) = e^{i2nz} \sin z \, \frac{e^{-\frac{x^2}{a}} (\cos z)^{\frac{1}{\beta}-1} \cosh\sqrt{-\frac{4b'x^2}{a^2}\ln(\cos z)}}{\sqrt{-\beta\pi \ln(\cos z)}} \tag{4.5.2}$$

on the contour $\mathcal{C}_1 \bigcup \mathcal{C}_2 \bigcup \mathcal{C}_3$ in the complex $z-$plane where

$$\mathcal{C}_1 = \{z = iy, 0 \le y \le T\}, \quad \mathcal{C}_2 = \left\{z = x + iT, 0 \le x \le \frac{\pi}{2}\right\},$$
$$\mathcal{C}_3 = \left\{z = \frac{\pi}{2} + iy, T \ge y \ge 0\right\}$$

and sending T to infinity. This contour is the steepest-decent curve that connects $z = 0$ and $z = \frac{\pi}{2}$. The detailed analysis for $I(z)$ will be shown in Appendix, which suggests that for large n, $|C_{2n}|$ is asymptotically proportional to

$$\cosh\left(\frac{2x\sqrt{b'}}{a}\sqrt{\ln n}\right) n^{-\frac{1}{\beta}} (\ln n)^{-\alpha} \tag{4.5.3}$$

where $\alpha = \frac{1}{2}$, 1 or $\frac{3}{2}$ depending on different values of x and β, which is shown in the Appendix. As a result, $\sum_{n=0}^{\infty} |C_n|$ converges for $\beta < 1$ for $x \neq 0$ and for $\beta \le 1$ when $x = 0$. And this serves as the criterion for the pointwise, uniform convergence of the series expansion for $f(\xi) = \sqrt{1-\xi^2} P_{x,t}(\xi) = \sum_{n=0}^{\infty} C_{2n} T_{2n}$ in [0, 1], due to the boundedness of Chebyshev polynomials in this interval.

Furthermore, from the relationship (3.5.2) between the Péclet number $\mathrm{Pe} = \frac{\sigma^2}{\kappa}$ and β, and the fact that β is an increasing function of time for fixed σ and κ, we conclude that $\mathrm{Pe} = 2$ is the critical value that distinguishes the pointwise convergence of the series reconstruction via the standard Chebyshev polynomials at all times. However, it can be easily verified that with the shifted Chebyshev polynomials, the series expansion converges for arbitrary (x, t) and Pe, by simply replacing $\frac{1}{\beta}$ with $\frac{1}{\beta} + 1$ in (4.5.3).

5. NUMERICAL RESULTS OF SERIES RECONSTRUCTION

5.1. Reconstruction via Extension to $[-1, 1]$ for $T_0(x) = e^{-x^2}$

First we carried out the reconstruction for the PDF (2.5) using series approximants

$$P_{x,t}(\xi) \approx \frac{\sum_{n=0}^{N-1} C_{2n} T_{2n}(\xi)}{\sqrt{1-\xi^2}} \tag{5.1.1}$$

by evenly extending it to $[-1, 1]$. The numerical results are illustrated in Fig. 1, which compares the exact PDF (solid line) with its series reconstruction (dashed line) obtained by setting $N = 4$ in (5.1.1) (first 4 even moments are used). Four reconstructions are done at $t = 1$ for different x and Pe values. We note that the similar case with an odd extension yields a nearly identical comparison.

The reconstructions in the upper two panels, in which $x = 0$ and $\mathrm{Pe} \le 2$, agree with the exact PDF with error near the singularity $\xi = 1$, respectively; while the two in the lower panels, in which $x \neq 0$, $\mathrm{Pe} = 2$ or $x = 0$, $\mathrm{Pe} > 2$, fail to recover

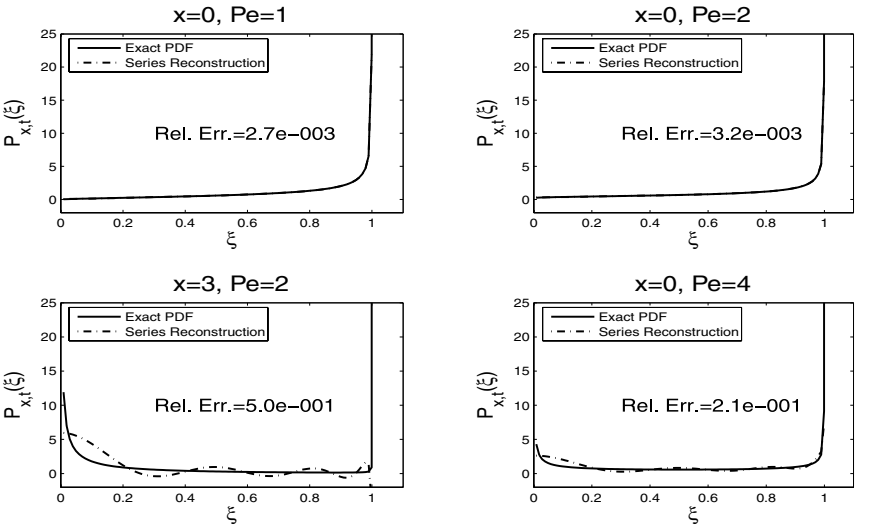

Fig. 1. 4-Term Chebyshev Reconstructions of the PDF at $t = 1$.

the true distributions almost everywhere. Recall that the series reconstruction is expected to fail whenever $P_{x,t}(0) = \infty$, since the truncated series (5.1.1) is always smooth at $\xi = 0$.

Does an increasing N help reducing the error? The answer is no. In the left panel of Fig. 2, we increase N to 40 and compare the series reconstruction using the standard Chebyshev polynomials to the exact PDF for $x = 2$, $t = 1$ and $\mathrm{Pe} = 4$. We can see the rapid oscillations near $\xi = 0$, which is a characteristic of high order polynomials in a finite interval, let alone the fact that to obtain the coefficients about 40 significant digits are required for accurate summation of Eq. (4.3.3). But an alternative polynomial family can improve the reconstruction. In the right panel, we reconstruct the PDF via shifted Chebyshev polynomials and

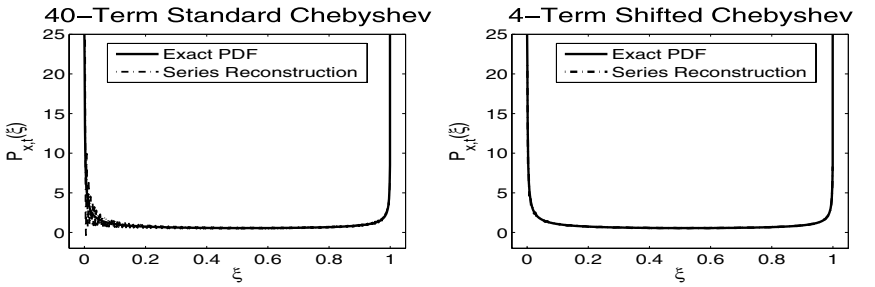

Fig. 2. Reconstructions of the PDF at $t = 1$ from Different Orthogonal Polynomials.

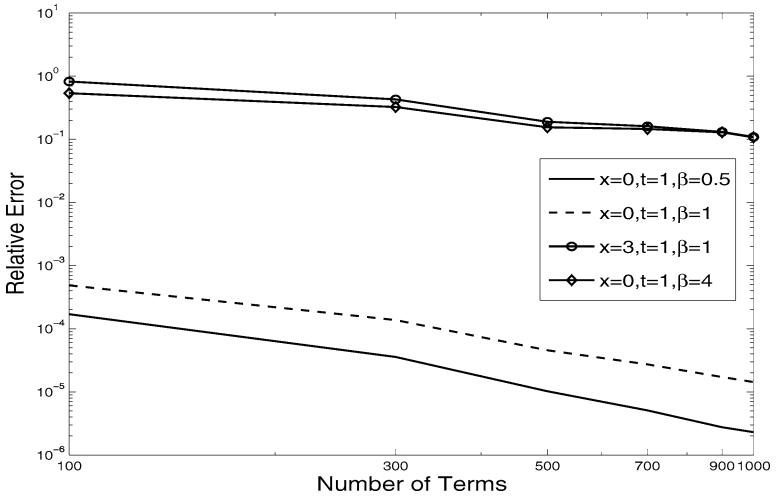

Fig. 3. The Relative Errors of Series Reconstructions VS Number of Terms Kept in (5.1.1).

re-define $r(\xi) = \sqrt{\xi^3(1-\xi)}$. Now only 4 terms are needed to approximate $P_{x,t}(\xi)$ with negligible error. We will discuss how and why alternative choices of $r(\xi)$ and the polynomial family improve the reconstruction later in this section.

Figure 3 further shows the slow convergence rate of the reconstructions with increasing N, the number of terms used in the series (5.1.1), although when $x = 0$, $\beta \leq 1$, the relative errors are much smaller (less than 1% when $N = 4$). Here the relative error is defined by

$$\varepsilon_N = \frac{\left\| P_{x,t}(\xi) - \dfrac{\sum_{n=0}^{N-1} C_{2n} T_{2n}(\xi)}{\sqrt{1-\xi^2}} \right\|_2}{\| P_{x,t}(\xi) \|_2}. \tag{5.1.2}$$

5.2. Improving Series Reconstruction

Let us see how alternative choices of $r(\xi)$ and the polynomial family improve the reconstruction. Letting $r(\xi) = \sqrt{\xi^3(1-\xi)}$ and $Q_n(\xi) = T_n^*(\xi)$ as discussed in Sec. 4.4, we can reconstruct the PDF with only 4 terms (first 4 moments are used), to achieve a relative error less than 1%, which is shown in Fig. 4, in contrast to the lower two panels in Fig. 1. The negligible errors suggest that the performance of the series reconstruction relies on the capability of $(r(\xi))^{-1}$ to recover the singularities in $P_{x,t}(\xi)$, since the numerator in (5.1.1) is always continuous in [0, 1]. For example, when $x \neq 0$ and $\beta \geq 1$, we know from (2.5)

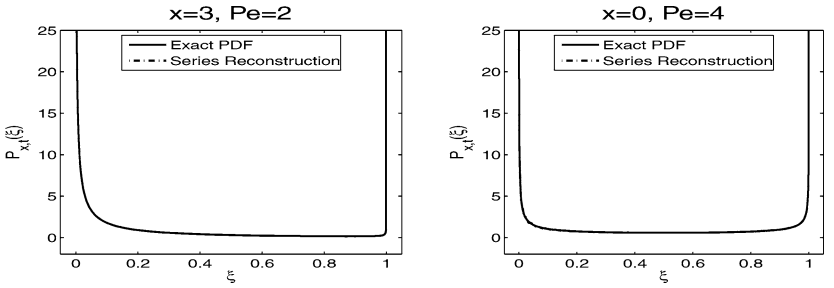

Fig. 4. 4-Term Shifted Chebyshev Reconstructions of the PDF at $t = 1$.

and Table 1 that $P_{x,t}(0) = P_{x,t}(1) = \infty$. Therefore $[r(\xi)]^{-1} = [\xi\sqrt{(1-\xi^2)}]^{-1}$, which has two singularities at $\xi = 0$ and 1, should be adopted instead of $[r(\xi)]^{-1} = [\sqrt{(1-\xi^2)}]^{-1}$. Of course, $r(\xi)$ should be defined in such a way that $r(\xi)w(\xi) = \xi^k$ where k is an non-negative integer and thus the coefficients can be computed using statistical moments as shown in (4.4.1). Figure 5 is a comparison between the convergence rates of reconstructing the same PDF using the following three different combinations of $r(\xi)$ and Q_n, each of which corresponds to one curve in either panel

1. Shifted Legendre polynomials defined on [0, 1] and $r(\xi) = \xi(1-\xi)$;
2. Shifted Chebyshev polynomials defined on [0, 1] and $r(\xi) = \sqrt{\xi^3(1-\xi)}$;
3. Standard Chebyshev polynomials defined on $[-1, 1]$ and $r(\xi) = \xi\sqrt{1-\xi^2}$.

In the left panel of Fig. 5, $x = 3$, $\mathrm{Pe} = 2$ and $t = 1$, so $P_{x,t}(0) = P_{x,t}(1) = \infty$; whereas on the right, $x = 0$, $\mathrm{Pe} = 2$ and $t = 1$, so $P_{x,t}(0) = 0$, $P_{x,t}(1) = \infty$. Notice that the number of singularities in $[r(\xi)]^{-1}$ is greater than (right) or equal to (left) that of the exact PDF (2.5) for all three choices. For both PDF's, shifted Chebyshev polynomials give the optimal results, with relative errors of $\sim$1% when only 8 moments are used. It should also be noted that when we under-estimate the number of singularities, the reconstructions from any of the three polynomial families converges very slowly. This is not surprising because as we mentioned in Sec. 3.4, $f(\xi^*) = r(\xi^*)P_{x,t}(\xi^*) = \infty$ for some $\xi^* \in [0, 1]$ when this occurs.

Figure 5 also shows that even when the correct singularities are built into $r(\xi)$, the reconstructions using standard Chebyshev polynomials via extension converges much more slowly than those without extension. Other than the fact that different regularization functions are used here, extensions should be avoided if possible since they may introduce non-smoothness of $f(\xi)$ at the interior point $\xi = 0$ which can affect the convergence rate. More detailed quantitative analysis on this will be addressed in our future work.

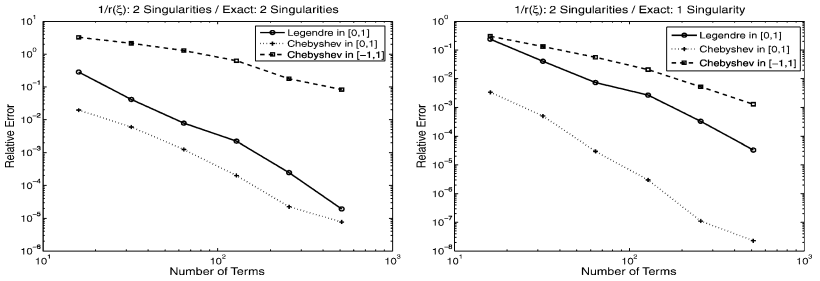

Fig. 5. Convergence Rates for Different $r(\xi)$ and $Q_n(\xi)$.

6. MONTE-CARLO SIMULATIONS AND PDF DYNAMICS

The purpose of this section is to study the effectiveness of Monte-Carlo methods applied in the problem (2.1), when the exact PDF for the tracer is known at all times. The Monte-Carlo simulation for Eq. (2.1) is straightforward by spectral methods, along with a simple random number generator. Moreover, at a fixed time t, the Monte-Carlo simulation for the tracer can be made easier by sampling $W(t)$ from a mean-zero Gaussian random variable with variance $\sigma^2 t$ from the scaling property of Wiener Processes. Nonetheless, to study the full temporal evolution of $P_{x,t}(\xi)$, one has to simulate the complete Wiener path $W(t)$, which is discretized as a sum of independent Gaussian random variables using standard techniques,[12] namely, $W(t) \simeq \sum_{i=0}^{N} dw_i$ where $dw_i \sim \mathcal{N}(0, \sigma^2 \Delta t_i)$.

For general stochastic flows and initial data, the analytic solution to the random advection-diffusion problem is not available as well as the exact scalar PDF. Monte-Carlo simulation is a powerful numerical tool to approximate the PDF and investigate its dynamics in such cases. Moreover, accurate Monte-Carlo simulations can be used to benchmark the performance of the PDF reconstructions via orthogonal polynomials discussed in the previous sections.

6.1. Uni-Modal Positive, Gaussian Initial Data $T_0(x) = e^{-x^2}$

We will first examine the case with the initial data $T_0(x) = e^{-x^2}$, for which we have the exact PDF (2.5) and exact moments (3.2.12) to evaluate the Monte-Carlo simulations. As we will see, the simulation does give an accurate approximation to the exact PDF and recover its spatio-temporal dynamics with a certain number of realizations.

6.1.1. Monte-Carlo Simulations

Figure 6 depicts the spatial structure of $P_{x,t}(\xi)$ obtained by two different approaches: exact formula (2.5) and Monte-Carlo simulations. Here Pe $= 2$ and

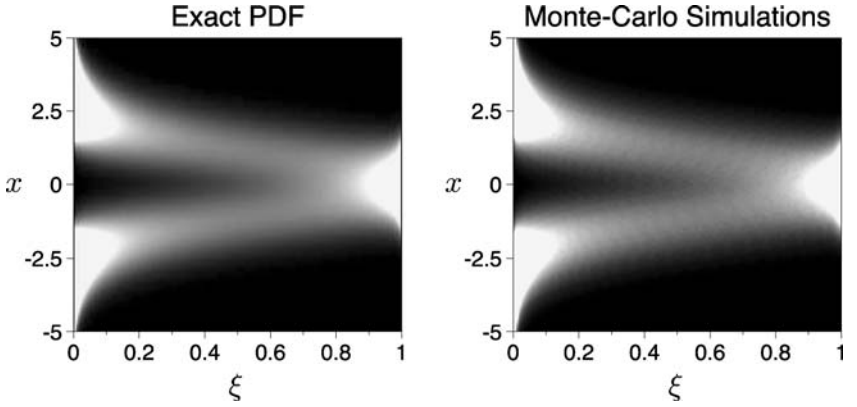

Fig. 6. Comparison Between the Exact PDF (2.5) and MC Simulations, Horizontal Axis—Renormalized Tracer ξ, Vertical Axis—Spatial Variable x, *: Grayscale ramp uniformly set in [0,2], same in all other grayscale figures.

$t = 1$. To obtain each histogram to simulate $P_{x,t=1}(\xi)$, 10^5 samples are drawn by the Monte-Carlo simulator and 100 bins are distributed uniformly between [0, 1]. Each panel is a snapshot of $P_{x,t}(\xi)$, exact on the left and Monte-Carlo simulated on the right, at time $t = 1$. The horizontal axis is the renormalized scalar ξ-axis, ranging from 0 to 1, and the vertical axis is the spatial x-axis between $[-5, 5]$. The grayscale ramp is set uniformly between [0, 2] such that regions where $P_{x,t}(\xi) \approx 0$ are dark, whereas bright regions implies $P_{x,t}(\xi) \gtrsim 2$. For example, if we take a horizontal slice of the left panel along $x = 3$, and interpret the brightness with corresponding numbers, we would recover the solid curve shown in the lower-left panel of Figure 1.

The overall agreement between the Monte-Carlo simulations and the exact PDF is obvious from Fig. 6. To benchmark quantitatively the performance of the Monte-Carlo simulator, we first compare the exact moments of the random variable ξ with the moments generated from the simulation histogram. A valid Monte-Carlo simulation should converge to the exact PDF as the numbers of realizations increases. Figure 7 is the summary of the two tests mentioned above, where $x = 2$, $\beta = 1$, $t = 1$ and 100 bins are used to construct the histograms. The relative error plotted in the right panel is defined similarly to Eq. (5.1.2) by replacing the series reconstruction with the simulated histogram.

In the left panel, we can see that the simulated moments coincide with the exact moments for $n \lesssim 1000$. The right panel depicts the L^2 relative error which shows improved convergence with the number of realizations increasing from 10^4 to 10^7.

With increasing M, the number of realizations, the relative error first decays like $\frac{1}{\sqrt{M}}$, while it remains almost the same for $M \geq 10^6$. We also find

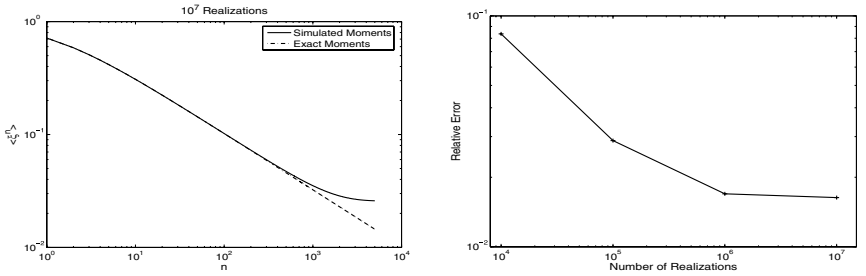

Fig. 7. Benchmarking the Monte-Carlo Simulator, Left: Exact Moments VS Simulated Moments, Right: Relative Error in $P_{x,t}(\xi)$ VS Number of Realizations.

that the pointwise relative error is negligible ($\sim 0.1\%$) when $M \geq 10^5$ everywhere in $[0, 1]$ except near the singularity $\xi = 1$. This error saturation is however inevitable with any simulation approach because of the systematic bias introduced by discretization errors, the finite statistics, histogram binning, etc.

6.1.2. Spatio-Temporal PDF Dynamics

We have seen that with 10^5 realizations (with L^2 relative error $\sim$1%), the Monte-Carlo simulation favorably reproduce measure, which serves as a tool to study more complicated PDF evolution for cases where the exact PDF is not available. As a test problem, first we present the dynamics associated with the exact PDF (2.5). For the deterministic heat equation, namely $\sigma = 0$, it is clear that $P_{x,t}(\xi) = \delta(\xi - e^{-x^2/b'})$ for any x and t, as we have seen in Sec. 2.5. But how does the random drift change the PDF dynamics? Figures 8 and 9 together offer a comprehensive illustration of the spatial-temporal structure of Monte-Carlo simulations of $P_{x,t}(\xi)$ when $\mathrm{Pe} = 2$. In both figures, different panels, which are the counterparts of the right panel in Fig. 6 at different times, form a time sequence showing the dynamical behavior of $P_{x,t}(\xi)$. Here replacing the Monte-Carlo simulations with the exact PDF will not change the dynamics at all since their relative difference is only about 1%. Initially at $t = 0$, for any (ξ, x), $P_{x,t=0}(\xi) = \delta(\xi - e^{-x^2})$ since the initial data is deterministic. That is, $P_{x,t=0}(\xi) = 0$ except on the curve (e^{-x^2}, x), which is the rotated Gaussian in the top-left panel in Fig. 8. Immediately after that, the random drift smears the deltas and we see a gray ribbon developing around the curve. Gradually, for any nonzero x, the majority of the probability will shift towards $\xi = 1$ since from Eq. (3.3.2), $P_{x,t}(\xi) \sim P_{0,t}(\xi)$ as $t \to \infty$, which has a singularity at $\xi = 1$. Moreover, from the panels $t = 0.08, 0.1, 0.25$ and 0.5 in Fig. 8, we conclude that for those x's in the core of the Gaussian, the probability shifts faster than for those in the tails of the Gaussian.

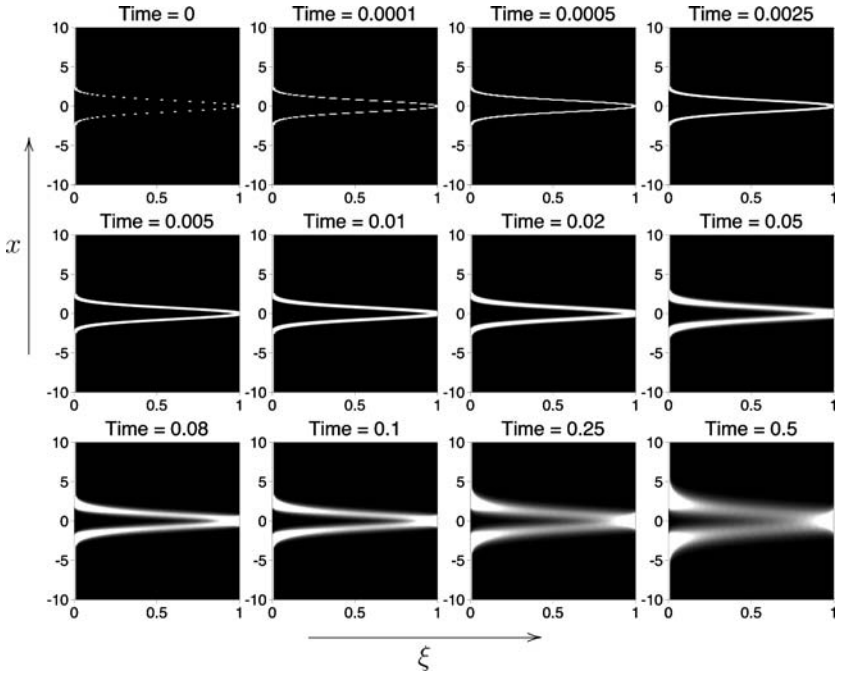

Fig. 8. The Short Time Dynamics of $P_{x,t}(\xi)$: from Gaussian to Ribbons.

This explains the emergence of:

1. Two bright, white regions at the junctions between the core and the tails of the initial Gaussian when $t = 0.5$. For these x values, the singularity in the initial delta function slowly begins to disappear and the probability "smears" around these junctions.
2. Two gray ribbons around the core region of the initial Gaussian when $t = 0.5$, in which the probability density is substantially greater than 0 (black) but not very large (white). For any fixed x within this region, the transient measure Eq. (2.5) is drastically different from the initial measure $\delta(\xi - e^{-x^2})$ and is converging to its long time asymptotic limit Eq. (3.1.3).
3. A bright, white region near $(\xi = 1, x = 0)$, within which $P_{x,t}(\xi) \approx P_{0,t}(\xi)$.

The time series shown in Fig. 8 continues in Fig. 9. Notice that two high density regions near $\xi = 0$ "moves away" from the line $x = 0$ towards large $|x|$ values. Eventually when $t = 500$, the initial Gaussian disappears completely. For $|x| \leq 10$, the brightness is almost homogeneous in x direction and we see only vertical stripes. This agrees with Eq. (3.3.2), namely, $P_{x,t}(\xi)$ is uniform in x when $t \to \infty$. However, this argument should be valid only over compact sets, since if we

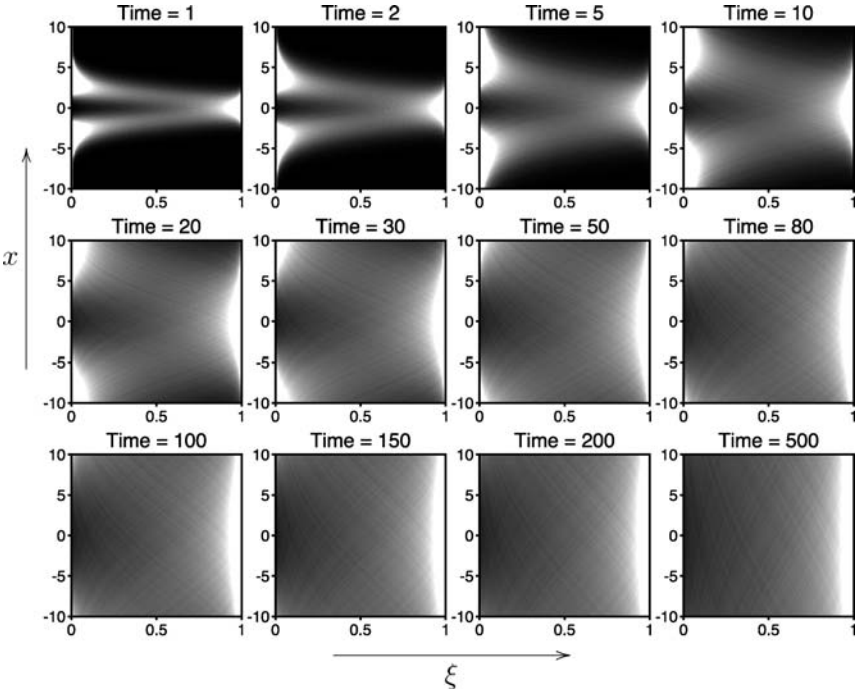

Fig. 9. The Long Time Dynamics of $P_{x,t}(\xi)$: from Ribbons to Stripes.

extend the plotted portion of x-axis, we will see the two bright, white regions again. In fact, this moving speed can be estimated here to be proportional to $1/\sqrt{t}$, which is ultimately attributed to the x^2/t self-similarity that we discussed in Sec. 3.3 and can be seen from Eq. (2.5). For general models with such behavior, one way to identify the speed is to find $|\tilde{x}|$ where $\tilde{x}$ maximizes $P_{x,t}(D)$ for some small number D as a function of t, which is approximately the $|x|$ value at the centers of the high density regions. At the spatial locations with larger $|x|$ values, $P_{x,t}(D)$ is smaller since the initial scalar profile concentrated near $x = 0$ has not yet arrived via diffusion. Thus the probability is confined in a very small interval with $\xi \ll D$, while for smaller $|x|$, $P_{x,t}(D)$ is also smaller since these locations are inside the core of the diffusing Gaussian and the probability accumulates near $\xi = 1$. Therefore, $\pm\tilde{x}$ can be regarded as the "fronts" of the averaged tracer concentration. Setting $D = 0.1$ and with time running from 1 to 10^6, we obtained Fig. 10. The interpretation of the slope $\sim$0.5 is that $\tilde{x}^2 \propto t$ and then the speed $d\tilde{x}/dt \propto 1/\sqrt{t}$. This confirms that the random solution (3.1.1) inherit the self-similarity from the pure heat equation. Essentially, for this simple random advection, the averaged tracer concentration is govern by a heat equation with an effective diffusivity computed by the Green-Kubo formula.

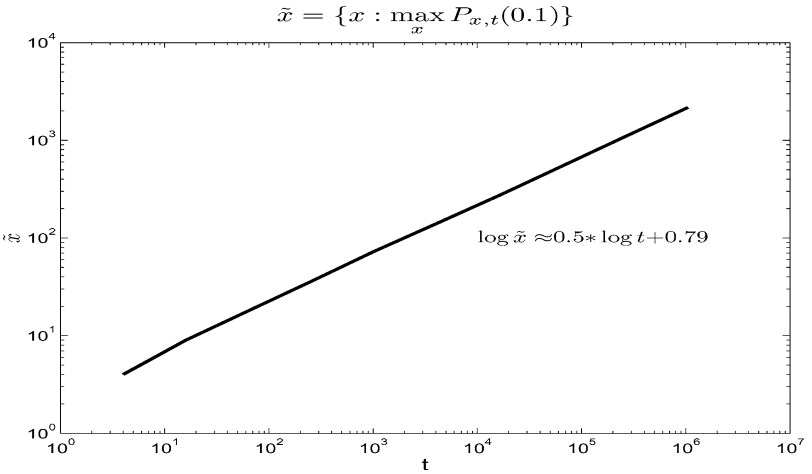

Fig. 10. The $|x|$ Value at the "Information Fronts" of VS Time.

6.1.3. Effects of the Péclet number

As we mentioned in Sec. 3.5, the Péclet number $\mathrm{Pe} = \frac{\sigma^2}{\kappa}$ dictates $P_{x,t}(\xi)$ at large times. Figure 11 demonstrates the spatio-temporal evolutions of $P_{x,t}(\xi)$ for different values of Pe. Recall that from Eqs. (2.5), (3.3.2) and (3.5.2),

$$\lim_{t\to\infty} P_{x,t}(\xi) = \lim_{t\to\infty} P_{0,t}(\xi) = \frac{\sqrt{2}\,\xi^{\frac{2}{\mathrm{Pe}}-1}}{\sqrt{\mathrm{Pe}\,\pi\,\ln\xi}} \tag{6.1.1}$$

where Pe characterizes the competition between the random drift and the diffusion. This is manifested in the $t = 500$ panels, in which more and more density shifts from near $\xi = 1$ and accumulates near $\xi = 0$ with increasing Pe, although the short-time PDF behaviors when $t < 0.5$ are similar for these four Pe values. This shift in the PDF is attributed to the fact that the higher Pe is, the more turbulent the flow is and therefore the higher probability the scalar has to access far-field, small values.

6.2. Bimodal Initial Data $T_0(x) = 2xe^{-x^2}$

For this initial data, the general exact PDF solution is not available. However, we can still solve the linear, random advection-diffusion problem (2.1) analytically, by simply taking the spatial derivative of (3.1.1) and the exact solution for $T_0(x) = 2xe^{-x^2} = -\frac{d}{dx}e^{-x^2}$ reads

$$T(x,t) = \frac{2(x - W(t))}{(1+4\kappa t)^{\frac{3}{2}}} \exp\left(-\frac{(x-W(t))^2}{1+4\kappa t}\right). \tag{6.2.1}$$

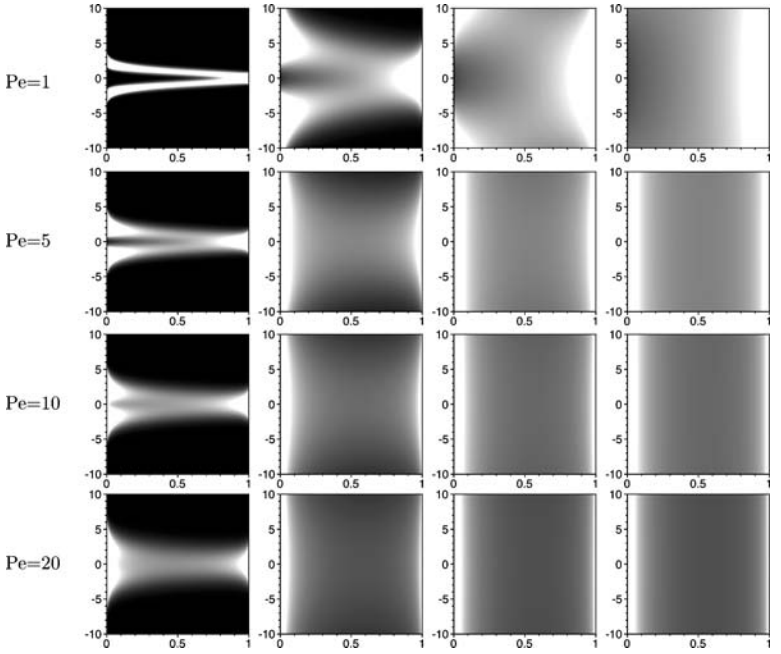

Fig. 11. Effects of the Péclet number for $T_0(x) = e^{-x^2}$.

which has two extrema (bimodal) in x-direction. Now we can re-define $T_{\max}(t) = \frac{\sqrt{2\,e^{-1}}}{4\kappa t+1}$ such that the random variable $\xi = \frac{T(x,t)}{T_{\max}(t)} \in [-1, 1]$ and its exact statistical moments are

$$\langle T^N \rangle_\gamma = \left(\frac{4a}{b'^2(aN+b')}\right)^{\frac{N}{2}} \frac{e^{-\frac{Nx^2}{b'} + \frac{\beta N^2 x^2}{aN+b'}}}{\sqrt{\pi(1+\beta N)}} \times \sum_{\substack{j=0, \\ \text{j even}}}^{N} \binom{N}{j} \left(\frac{x}{\sqrt{a(1+\beta N)}}\right)^{N-j} \Gamma\left(\frac{j+1}{2}\right). \tag{6.2.2}$$

from similar calculations as in Eq. (3.2.9).

Although in this case, the exact PDF is not available by performing inverse Laplace transform as shown in Sec. 3.4, we are able to find the space-independent, limit distribution $P_\infty(\xi)$ as $t \to \infty$ as follows. First, the long time asymptotic moments are

$$\langle \xi^N \rangle_\gamma \sim \frac{1+(-1)^N}{2} \left(\frac{e\ \mathrm{Pe}}{1+PeN/2}\right)^{\frac{N}{2}} \frac{\Gamma(\frac{1+N}{2})}{\sqrt{\pi(1+PeN/2)}}. \tag{6.2.3}$$

Notice that this is not in the form of Eq. (3.3.2) because $\hat{T}_0(0) = 0$. These moments are reminiscent of formulas involving the Lambert W- or tree functions,[11] which provides a generating function for the number of rooted trees on n points. Using this observation we have been able to explicitly compute the distribution in terms of the tree function as follows: If we define the functions $w_i(\xi),\ i = -1,\ 0$ for any $\xi \in [0, 1]$ by

$$w_i\, e^{1-w_i} = x, \qquad w_{-1}(1) = w_0(1) = 1, \qquad w_0(0) = 0 \text{ and } w_{-1}(0) = \infty \quad (6.2.4)$$

we have

$$\begin{aligned}
&\frac{1}{\sqrt{e\pi\,\mathrm{Pe}}} \int_{-1}^{1} \xi^N \left(\frac{e^{\frac{\mathrm{Pe}-2}{2\mathrm{Pe}} w_0(\xi^2)}}{1 - w_0(\xi^2)} - \frac{e^{\frac{\mathrm{Pe}-2}{2\mathrm{Pe}} w_{-1}(\xi^2)}}{1 - w_{-1}(\xi^2)} \right) d\xi \\
&\quad = \frac{1 + (-1)^N}{2\sqrt{e\pi\,\mathrm{Pe}}} \left(\int_0^1 x^{\frac{N-1}{2}} \frac{e^{\frac{\mathrm{Pe}-2}{2\mathrm{Pe}} w_0(x)}}{1 - w_0(x)}\, dx - \int_0^1 x^{\frac{N-1}{2}} \frac{e^{\frac{\mathrm{Pe}-2}{2\mathrm{Pe}} w_{-1}(x)}}{1 - w_{-1}(x)}\, dx \right) \\
&\quad = \frac{1 + (-1)^N}{2\sqrt{e\pi\,\mathrm{Pe}}} \int_0^\infty w^{\frac{N-1}{2}} e^{\frac{N+1}{2}(1-w) + \frac{\mathrm{Pe}-2}{2\mathrm{Pe}} w} dw \\
&\quad = \frac{1 + (-1)^N}{2} \left(\frac{e\ \mathrm{Pe}}{1 + \mathrm{PeN}/2} \right)^{\frac{N}{2}} \frac{\Gamma\left(\frac{1+N}{2}\right)}{\sqrt{\pi(1 + PeN/2)}}
\end{aligned} \quad (6.2.5)$$

in which we introduce the changes of variable $\xi = \sqrt{x}$ and $x = we^{1-w}$. Therefore,

$$P_\infty(\xi) = \frac{e^{\frac{\mathrm{Pe}-2}{2\mathrm{Pe}} w_0(\xi^2)}}{1 - w_0(\xi^2)} - \frac{e^{\frac{\mathrm{Pe}-2}{2\mathrm{Pe}} w_{-1}(\xi^2)}}{1 - w_{-1}(\xi^2)}, \quad \xi \in (-1, 1). \quad (6.2.6)$$

Further, the singular limits of the PDF as ξ approaches 0 and ± 1 are

$$\begin{aligned}
&\lim_{\xi \to (-1)^+, 1^-} \frac{e^{\frac{\mathrm{Pe}-2}{2\mathrm{Pe}} w_0(\xi^2)}}{1 - w_0(\xi^2)} - \frac{e^{\frac{\mathrm{Pe}-2}{2\mathrm{Pe}} w_{-1}(\xi^2)}}{1 - w_{-1}(\xi^2)} = \lim_{\varepsilon \to 0^+} \frac{e^{\frac{\mathrm{Pe}-2}{2\mathrm{Pe}}(1-\varepsilon)}}{\varepsilon} - \frac{e^{\frac{\mathrm{Pe}-2}{2\mathrm{Pe}}(1+\varepsilon)}}{-\varepsilon} = +\infty \\
&\lim_{\xi \to 0^+, 0^-} \frac{e^{\frac{\mathrm{Pe}-2}{2\mathrm{Pe}} w_0(\xi^2)}}{1 - w_0(\xi^2)} - \frac{e^{\frac{\mathrm{Pe}-2}{2\mathrm{Pe}} w_{-1}(\xi^2)}}{1 - w_{-1}(\xi^2)} = \lim_{\varepsilon \to 0^+} \frac{e^{\frac{\mathrm{Pe}-2}{2\mathrm{Pe}} \varepsilon}}{1 - \varepsilon} - \frac{\varepsilon e^{\frac{\mathrm{Pe}-2}{2\varepsilon\mathrm{Pe}}}}{\varepsilon - 1} = \begin{cases} 1, & \mathrm{Pe} \le 2 \\ +\infty, & \mathrm{Pe} > 2 \end{cases}.
\end{aligned} \quad (6.2.7)$$

So again, from the series reconstruction perspective, $\mathrm{Pe} = 2$ is the critical value. Also, when $\mathrm{Pe} > 2$, the scalar has a much higher probability of being near 0 due to a singularity.

Figure 12 through 15 are the Monte-Carlo simulations that illustrate the spatio-temporal dynamics of $P_{x,t}(\xi)$ with $T_0(x) = 2xe^{-x^2}$. Similar to the PDF evolution shown in Figs. 8 and 9, the initial Dirac mass supported by the curve $(\sqrt{2e}xe^{-x^2},\ x)$ is smeared as time advances. We observe that the smearing is symmetric with respect to the origin in the $x - \xi$ plane, due to the symmetry of

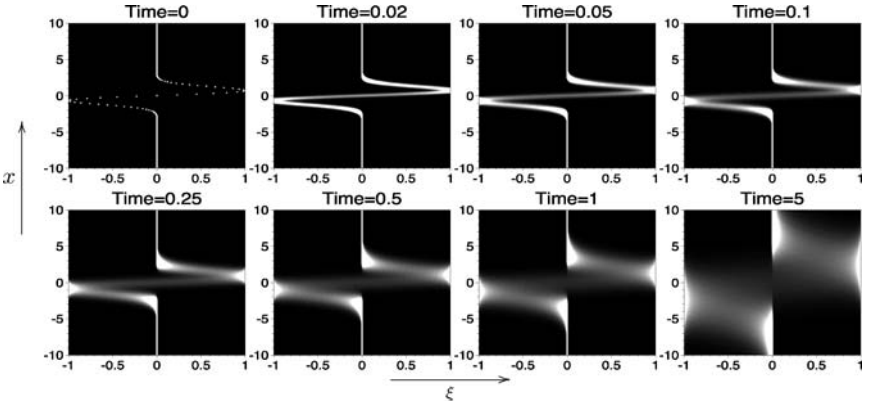

Fig. 12. The PDF Dynamics of $P_{x,t}(\xi)$ with $T_0(x) = 2xe^{-x^2}$ where Pe $= 2$.

the initial profile and the x-independence of the random drift. Also, four high density regions emerge near $\xi = 0$ and $\xi = \pm 1$. For Pe $= 4$, the high density regions near $\xi = 0$ remains for all x's at $t > 1$, whereas they vanishes for Pe $= 2$. Figures 12 and 13 also suggest that at the edges of the high density regions near $\xi = 0$, if we fix x, there seems to be a "jump discontinuity" in the PDF at $\xi = 0$, where the grayscale changes abruptly from dark to bright. This is different from the singularities as we see where $P_{x,t}(\xi) = \infty$ and it is most noticeable in the $t = 1, 5$ panels in Fig. 12 and $t = 0.25, 0.5$ panels in Fig. 13. Figure 14 is an illustration of such a phenomena at $x = 2.5$, $t = 1$ for Pe $= 2$, which is essentially a horizontal slice of the "Time=1" panel in Fig. 12. The rigorous analysis for this phenomena is an open question since the exact PDF is not available. An intuitive

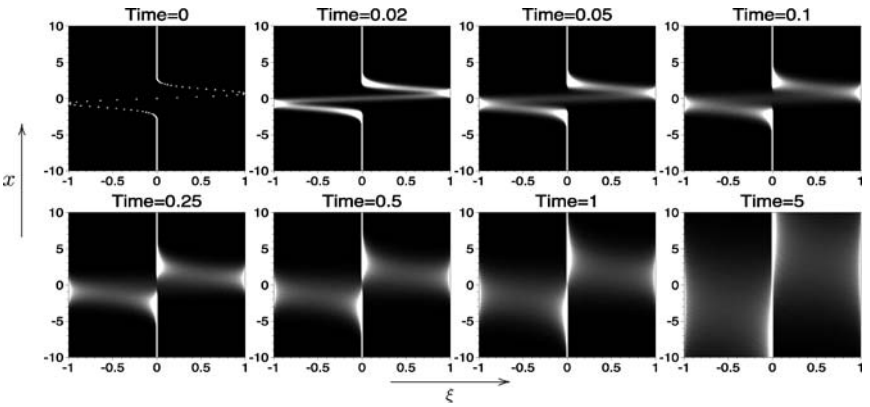

Fig. 13. The PDF Dynamics of $P_{x,t}(\xi)$ with $T_0(x) = 2xe^{-x^2}$ where Pe $= 4$.

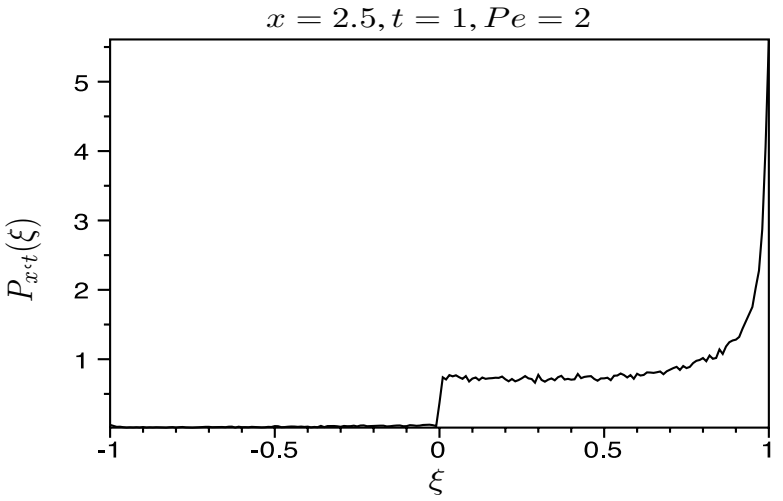

Fig. 14. "Jump Discontinuity" of $P_{x,t}(\xi)$ with $T_0(x) = 2xe^{-x^2}$.

explanation can be made since the initial tracer field $T_0 = 2xe^{-x^2}$ has a positive bump near $x = 2.5$, which is translated by random advection and is smoothed by molecular diffusion as time advances. But by $t = 1$, the tracer at these locations will remain positive, often small, unless the initial field is randomly translated so far away that the tracer can admit negative values which are initially located at $x < 0$. Such a rare, large deviation has a probability much smaller than that of the realizations producing a positive scalar at $(x = 2.5, t = 1)$, which leads to a jump discontinuity in the tracer PDF at $\xi = 0$.

Eventually at $t = 1000$, we see in Fig. 15 three high density, vertical stripes, near $\xi = 0$ and $\xi = \pm 1$ respectively, for Pe $= 4$, whereas only two such stripes exist near $\xi = \pm 1$ for Pe $= 2$.

The formula (6.2.3) also allows us to perform series reconstructions using the moments as discussed in Sec. 3, with which we compare the Monte-Carlo simulations in Fig. 16 and two approximations exhibit favorable agreement. Here we employ standard Chebyshev polynomials to reconstruct the PDF and we set $r(\xi) = \sqrt{1 - \xi^2}$ for Pe $= 2$ and $r(\xi) = \xi\sqrt{1 - \xi^2}$ for Pe $= 4$. And the extensions discussed in Sec. 3.3 is not required here because $\xi \in [-1, 1]$. In Fig. 16, the limit distributions $P_\infty(\xi)$ are not plotted since it overlaps completely with the series reconstructions.

6.3. Bimodal, Positive Initial Data $T_0(x) = e^{-(x-A)^2} + e^{-(x+A)^2}$

For this initial data, which is a sum of two Gaussians, the exact PDF solution is not available, although the corresponding random advection-diffusion problem (2.1) can again be solved analytically since it is linear. Moreover, we can obtain

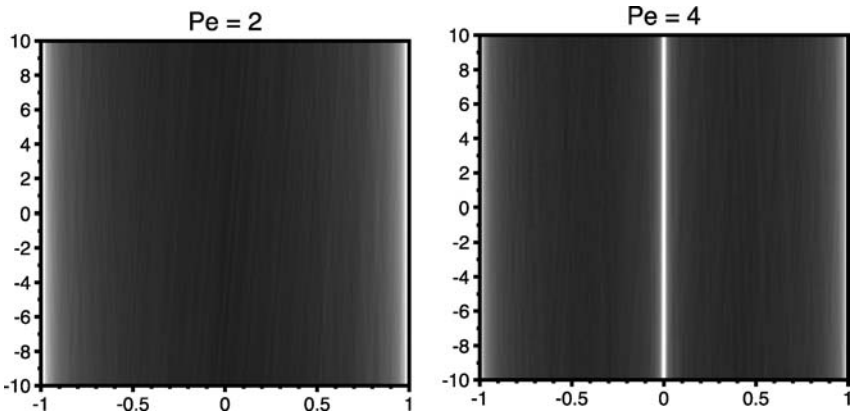

Fig. 15. Monte-Carlo Simulations for $P_{x,t}(\xi)$ with $T_0(x) = 2xe^{-x^2}$ at $t = 1000$.

the exact moments for the renormalized scalar utilizing Eq. (3.2.10)

$$\langle \xi^N \rangle_\gamma = \frac{2^{-N}}{\sqrt{1+\frac{a}{b'}N}} \exp\left(-\frac{N\pi^2(x+A)^2}{aN+b'}\right) \sum_{j=0}^{N} \binom{N}{j} \times \exp\left(\frac{4\pi^2 Aj[aA(j-N)+bx]}{b'(aN+b')}\right). \tag{6.3.1}$$

It is obvious that in the long time limit $\langle \xi^N \rangle_\gamma \sim (1+\frac{\mathrm{Pe}}{2}N)^{-\frac{1}{2}}$ and thus the PDF is asymptotically equal to $P_{0,t}(\xi)$ for the uni-modal, Gaussian data $T_0(x) = e^{-x^2}$ from Eq. (3.2.12). In fact, this has been discussed in Sec. 3.3, since for large times $b = 4\kappa t \sim 4\kappa t + 1 = b'$ and therefore the PDFs for $T_0(x) = e^{-x^2}$ ($\hat{T}_0(0) \neq 0$) and $T_0(x) = \delta(x)$ are asymptotically equal to each other.

The short time PDF dynamics for this initial data has a unique feature different than the two cases we have seen in Secs. 5.1 and 5.2 — another singularity emerges

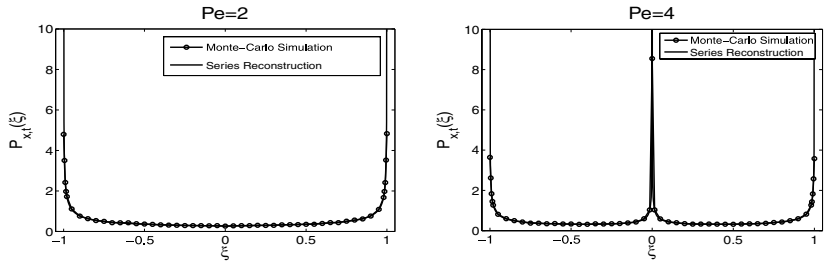

Fig. 16. 10-Term Series Approximations of $P_{0,t}(\xi)$ with $T_0(x) = -2\,xe^{-x^2}$ at $t = 1000$.

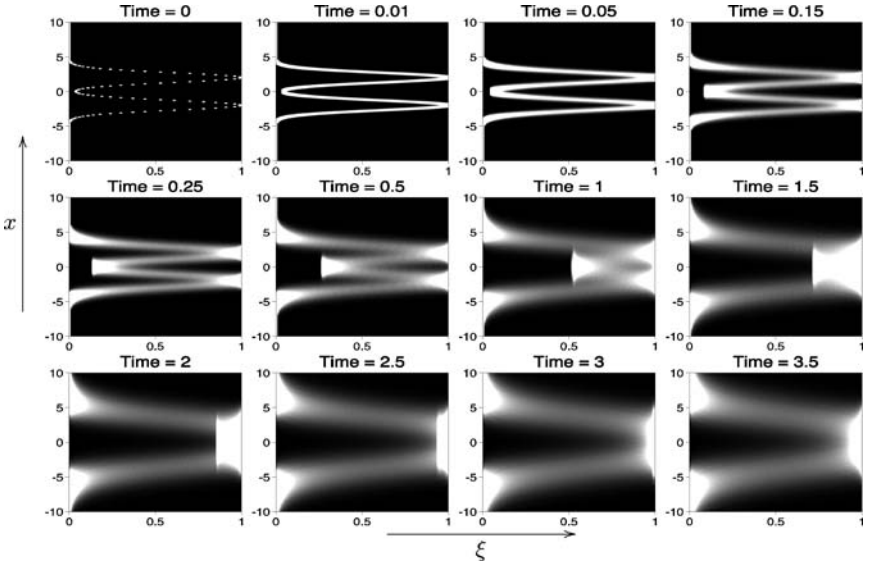

Fig. 17. Short Time PDF Dynamics for $T_0(x) = e^{-(x-2)^2} + e^{-(x+2)^2}$.

besides the ones at $\xi = 0,\ 1$. This is illustrated in Fig. 17. We can see from the figure that a singularity near $x = 0$ moves towards $\xi = 1$ as time increases and eventually merges with the singularity at $\xi = 1$. It is easy to check numerically that the ξ value at this singularity is approximately the corresponding pure heat solution at $x = 0$, which is a local minimum. This minimum becomes a maximum at a later time so it will merge with the maximum at $\xi = 1$ at later times. In light of this observation, next we present an explanation of why the singularities of $P_{x,t}(\xi)$ can only appear at the extrema of the renormalized pure heat solution.

6.4. Identifying the Singularities in $P_{x,t}(\xi)$

Now we show that, *at time t, if* $(x^*, \xi^* = \frac{T(x^*,t)}{T_{\max}(t)})$ *with* $|x^*| < \infty$ *is a critical point, namely,* $\frac{\partial}{\partial x}(\frac{T(x^*,t)}{T_{\max}(t)})|_{x=x^*} = 0$, *then* $P_{x,t}(\xi^*) = \infty$ *for any x, provided that* $\frac{T(x,t)}{T_{\max}(t)}$ *is differentiable in x and satisfies the Lipshitz condition locally*. To see this, we consider

$$p(\varepsilon) := \text{Prob}\left(\left|\frac{T(x^*,t)}{T_{\max}(t)} - \xi^*\right| < \varepsilon\right) = \int_I P_{x,t}(\xi)\, d\xi \tag{6.4.1}$$

for any small $\varepsilon > 0$, where the integration interval $I = [\xi^* - \varepsilon, \xi^* + \varepsilon] \cap [0, 1]$. Thus $P_{x,t}(\xi^*) = \infty$ if and only if $\lim_{\varepsilon \downarrow 0} \frac{\varepsilon}{p(\varepsilon)} = 0$. Notice that for the same ξ^*,

there can be multiple x^*'s such that $\frac{T(x^*,t)}{T_{\max}(t)} = \xi^*$, but it suffices to consider the case where there is only one such x^* because we will see that we only need a lower bound for $p(\varepsilon)$ here.

Next we take the Taylor expansion of renormalized, random solution near (x^*, ξ^*). For the test problem (2.1), we can simply expand the pure heat solution, which is just a rigid translation of the random solution (3.2.1), and then replace x by $x - W(t)$. It is clear that when $|x - W(t) - x^*|$ is small, the renormalized random tracer satisfies

$$\left| \frac{T(x^*, t)}{T_{\max}(t)} - \xi^* \right| \leq K_{x^*} |x - W(t) - x^*|^p \tag{6.4.2}$$

for some constant $p > 1$ and $K_{x^*} > 0$ determined by x^*, since (x^*, ξ^*) is a critical point. Therefore $K_{x^*}|x - W(t) - x^*|^p < \varepsilon$ implies $|\frac{T(x^*,t)}{T_{\max}(t)} - \xi^*| < \varepsilon$ and consequently, $\text{Prob}(K_{x^*}|x - W(t) - x^*|^p < \varepsilon) \leq p(\varepsilon)$. The probability on the left hand side of the inequality can be shown to be $O(\varepsilon^{1/p})$, via evaluating an elementary Gaussian integral. Thus $\lim_{\varepsilon \downarrow 0} \frac{\varepsilon}{p(\varepsilon)} = 0$.

However, the above arguments do not apply to $\xi^* = 0$, the heat solution at $|x| = \infty$, since we do not have local Taylor expansions at infinity. They also fails when there are infinitely many x^*'s such that $\frac{T(x^*,t)}{T_{\max}(t)} = \xi^*$ and any (x^*, ξ^*) is not a critical point. Moreover, the question of whether such singularities at critical points exist in more complicated turbulent flows, where the solution is not just a random translation of the pure heat solution, remains open for further study.

7. EXTENDED MODEL WITH A SOURCE TERM

Many geophysical problems are characterized not just by transport and diffusion, but also involve strong external sources, either through scalar production or destruction.[21,27] In the present calculation, to understand the role of such phenomena, scalar sources can be modeled with the addition of a scalar, deterministic, steady forcing function, $\Phi(x)$, and the governing equation for the scalar (2.1) becomes

$$\frac{\partial T}{\partial t} + \gamma(t)\frac{\partial T}{\partial x} = \kappa \frac{\partial^2 T}{\partial x^2} + \Phi(x) \tag{7.1}$$

It is interesting to compare the long time spatial distributions with and without the random white wind field. To have a finite long time limit, it is essential that the source function have spatial mean zero, namely, $\int_{-\infty}^{\infty} \Phi(x)dx = 0$.

The long time asymptotic solution, assumed to be non-zero, is given by

$$T_\infty^\omega(x) = \lim_{t\to\infty} \int_{-\infty}^{\infty} e^{2\pi ikx}\hat{\Phi}(k)\left[\int_0^t e^{-4\pi^2k^2\kappa s - 2\pi ikW(s)}ds\right]dk$$
$$= \int_{-\infty}^{\infty} e^{2\pi ikx}\,\widehat{T_\infty^\omega}(k)\,dk \tag{7.2}$$

where $\hat{\Phi}(k)$ is the Fourier transform of $\Phi(x)$. Notice that the effect of the initial data vanishes since it decays to 0 at long time. If the random advection were absent (the deterministic analogue), namely $\gamma(t) \equiv 0$, it is easy to verify that

$$\widehat{T_\infty}(k) = \frac{\hat{\Phi}(k)}{4\pi^2k^2\kappa} \tag{7.3}$$

Now we consider the mean of the random field T_∞^ω in the presence of the white wind

$$\langle\widehat{T_\infty^\omega}(k)\rangle = \hat{\Phi}(k)\lim_{t\to\infty}\int_0^t e^{-4\pi^2k^2\kappa s}\langle e^{-2\pi ikW(s)}\rangle\,ds = \frac{\hat{\Phi}(k)}{4\pi^2k^2(\kappa+\frac{\sigma^2}{2})} \tag{7.4}$$

according to Eq. (7.2). This is just the counterpart of its deterministic version (7.3) by replacing κ with the effective diffusivity $\kappa + \frac{\sigma^2}{2}$, namely,

$$\frac{\langle T_\infty^\omega(x)\rangle}{T_\infty(x)} = \frac{\langle\widehat{T_\infty^\omega}(k)\rangle}{\widehat{T_\infty}(k)} = \frac{1}{1+\frac{\mathrm{Pe}}{2}}. \tag{7.5}$$

This shows that the effect of the white wind on a sourced passive scalar equation always leads to a long time spatial distribution with mean values smaller than the deterministic counterpart, with an explicit, Péclet-dependent reduction.

Next we compare the mean of the two-point correlator of the random field in Fourier domain, $\langle\widehat{T_\infty^{\omega,2}}(j,k)\rangle$, with that of its deterministic analogue, $\widehat{T_\infty^2}(j,k)$. To recover the second moment of the random field, we only need to perform the two-dimensional inverse transform

$$\left\langle[T_\infty^\omega(x)]^2\right\rangle = \int_{\mathbb{R}^2} e^{2\pi i(j+k)x}\left\langle\widehat{T_\infty^{\omega,2}}(j,k)\right\rangle dj\,dk \tag{7.6}$$

and likewise for $T_\infty^2(x)$. Explicit integrations over simplices in $\mathbb{R}^2$ yield

$$\left|\frac{\langle\widehat{T_\infty^{\omega,2}}(j,k)\rangle}{\widehat{T_\infty^2}(j,k)}\right| = \frac{1}{1+\frac{\mathrm{Pe}}{2}}\,\frac{1}{1+\frac{\mathrm{Pe}}{2}\frac{(j+k)^2}{j^2+k^2}} < \frac{1}{1+\frac{\mathrm{Pe}}{2}} \tag{7.7}$$

for finite Pe, that is, the magnitude of each Fourier component of the second moment is also reduced in the presence of the random wind, with a similar Pe

dependent reduction. We also generalize these calculations for the higher order moments of the random field: T_∞^ω

$$\left\langle \widehat{T_\infty^{\omega,N}}(k_1,\ldots,k_N)\right\rangle = (4\pi^2)^{-N}\prod_{i=1}^{N}\hat{\Phi}(k_i)$$
$$\times \sum_{p_1,\ldots,p_N}\left[\prod_{i=1}^{N}\left(\kappa\sum_{j=1}^{i}k_{p_j}^2+\frac{\sigma^2}{2}\left(\sum_{j=1}^{i}k_{p_j}\right)^2\right)\right]^{-1} \tag{7.8}$$

where $\{p_1, p_2, \ldots, p_N\}$ is any permutation of $\{1, 2, \ldots, N\}$. These preliminary results indicate a non-trivial distribution and we will explore more thoroughly in future work.

8. CONCLUSIONS AND FUTURE WORK

We have explored the probability measures for a renormalized passive scalar diffusing in the presence of a random, Gaussian, white in time, wind field using a combination of tools. For initial data which is a single pure Gaussian profile, we are able to explicitly calculate in closed form the complete spatio-temporal probability measure. This is of great value in understanding the procedure for re-summing a measure from its statistical moments in that it provides an exact test problem, and further provides a mean to calculate directly asymptotic convergence rates for the reconstruction. For more general initial data, explicit calculations are not generally available, and we utilized well benchmarked orthogonal polynomial expansions and Monte-Carlo simulations for the reconstruction. For the bimodal initial data corresponding to the spatial derivative of a single Gaussian, we are able to explicitly calculate the exact long time asymptotic PDF, which was also useful in validating the Monte-Carlo simulations. For initial data comprised of a sum of spatial Gaussians, we employed Monte-Carlo simulation which documented the possibility of an interior singularity in the probability density function.

This elementary model provides a clear picture for the role in which the Péclet number plays in adjusting the spatio-temporal structure of the probability measure. Specifically, these calculations show a clear transition between the pure heat decay problem, which corresponds to a Dirac mass located at the heat solution, $\delta(\xi - e^{-x^2/(4\kappa t)})$, and the pure advection case which formally is recognized as the singular limit of infinite Péclet number, corresponding to the Dirac mass $\delta(\xi)$. In such a case at large times, any observer at a fixed location is almost sure to be far from the center of where the initial distribution has been shifted. Between these

two extreme cases, there is a balance between diffusion and advection, and the calculations provide the explicit measures depicting this balance.

These studies provide solid benchmarking for future studies involving more complicated fluid flows for which only a finite number of a statistical moments may be available. In such cases, we can approximate the probability measures of the random quantity with orthogonal polynomial expansions without the knowledge of the exact PDF.

APPENDIX

A.1. The Proof for Eq. (3.2.9)

By straightforward inductions, the formula for the characteristic polynomial of A_N reads

$$P_N(\lambda) = \pi^{2N}(\lambda - b)^{N-1}(\lambda - Na - b) \tag{A.1}$$

The eigenvector associated with the non-degenerate eigenvalue $\pi^2(Na + b)$ of A_N defined in (3.2.5) is explicitly $\vec{v}_N = \{\frac{1}{\sqrt{N}}, \frac{1}{\sqrt{N}}, \ldots, \frac{1}{\sqrt{N}}\}^t$, on account of the elementary matrix vector product for this eigenvector $A_N\vec{v}_N = \pi^2(Na + b)\vec{v}_N$. Therefore in Eq. (3.2.9)

$$V_m = \sum_{n=1}^{N} v_{mn} = \sqrt{N}\vec{v}_m^{\,t} \cdot \vec{v}_N = \begin{cases} 0, & \mathrm{m} \neq \mathrm{N} \\ \sqrt{N}, & \mathrm{m} = \mathrm{N} \end{cases} \tag{A.2}$$

since when $m \neq N$, $\vec{v}_m$ are eigenvectors associated with the multiple eigenvalue $\pi^2 b$.

A.2. Detailed Asymptotic Analysis for Expansion Coefficients C_n

Integrating $I(z)$ defined in (4.5.2) on $\mathcal{C}_1$ defined in Sec. 4.5 for large n, we have

$$\lim_{T\to\infty} \int_{\mathcal{C}_1} e^{i2nz} \sin z \, \frac{e^{-\frac{x^2}{a}} \, (\cos z)^{\frac{1}{\beta}-1} \, \cosh\sqrt{-\frac{4x^2b'}{a^2}\ln(\cos z)}}{\sqrt{-\beta\pi \ln(\cos z)}} \, dz$$

$$= -ie^{-\frac{x^2}{a}} \int_0^\infty \frac{e^{-2ny} \, \sinh y \, (\cosh y)^{\frac{1}{\beta}-1} \, \cos\sqrt{\frac{4x^2b'}{a^2}\ln(\cosh y)}}{\sqrt{\beta\pi \ln(\cosh y)}} \, dy \tag{A.8}$$

which is purely imaginary since $\ln(\cosh y)$ is non-negative. Clearly, the contribution from $\mathcal{C}_2$ is bound to vanish as $T \to \infty$. Finally, on $\mathcal{C}_3$, for large n,

$$\begin{aligned}
&\lim_{T\to\infty} \int_{\mathcal{C}_3} e^{i2nz} \sin z \; \frac{e^{-\frac{x^2}{a}} \, (\cos z)^{\frac{1}{\beta}-1} \, \cosh\sqrt{-\frac{4x^2b'}{a^2}\ln(\cos z)}}{\sqrt{-\beta\pi \, \ln(\cos z)}} \, dz \\
&= \frac{e^{-\frac{x^2}{a} - i(\frac{\pi}{2\beta} - n\pi)}}{\sqrt{\beta\pi}} \int_0^\infty \frac{e^{-2ny} \cosh y \, (\sinh y)^{\frac{1}{\beta}-1} \cosh\sqrt{-\frac{4x^2b'}{a^2}\ln(-i\sinh y)}}{\sqrt{-\ln(-i\sinh y)}} \, dy \\
&\sim \frac{(-1)^n e^{-\frac{x^2}{a} - i\frac{\pi}{2\beta}}}{\sqrt{\beta\pi}} \int_0^\varepsilon \frac{e^{-2ny} \cosh y \, (\sinh y)^{\frac{1}{\beta}-1} \cosh\sqrt{-\frac{4x^2b'}{a^2}\ln(-i\sinh y)}}{\sqrt{-\ln(-i\sinh y)}} \, dy
\end{aligned} \tag{A.9}$$

for $1 \gg \varepsilon > 0$ fixed since

$$\left| \int_\varepsilon^\infty \frac{e^{-2ny} \, \cosh y \, (\sinh y)^{\frac{1}{\beta}-1} \, \cosh\sqrt{-\frac{4x^2b'}{a^2}\ln(-i\sinh y)}}{\sqrt{-\ln(-i\sinh y)}} \, dy \right| < K_\varepsilon e^{-2n\varepsilon} \tag{A.10}$$

where K_ε is a constant determined by ε and and we will see that this is negligible compared to the contribution from the interval $[0, \varepsilon]$ for large n. Moreover, the last integral in (A.9) can be asymptotically approximated by

$$(-1)^n \sqrt{\frac{1}{\beta\pi}} \, e^{-\frac{x^2}{a} - i\frac{\pi}{2\beta}} \int_0^\varepsilon \frac{e^{-2ny} \cosh\sqrt{-\frac{4x^2b'}{a^2}\ln(-iy)} \, y^{\frac{1}{\beta}-1}}{\sqrt{-\ln(-iy)}} \, dy \tag{A.11}$$

since for $0 \le y \le \varepsilon$, $\cosh y \sim 1$ and $\sinh y \sim y$. Further, the contribution from the interval $[0, n^{-3/2}]$ in (A.11) is bounded by

$$\begin{aligned}
&\left| \int_0^{n^{-3/2}} \frac{e^{-2ny} \cosh\sqrt{-\frac{4x^2b'}{a^2}(\ln(-iy)} \, y^{\frac{1}{\beta}-1}}{\sqrt{-\ln(-iy)}} \, dy \right| \\
&< K \int_0^{n^{-3/2}} \frac{\exp\sqrt{-\frac{4x^2b'}{a^2}\ln y}}{\sqrt{-\ln y}} \, y^{\frac{1}{\beta}-1} \, dy \\
&= \widetilde{K} \left[1 - \mathrm{Erf}\left(\sqrt{\frac{3\ln n}{2\beta}} - \sqrt{\frac{\beta x^2 b'}{a^2}} \right) \right]
\end{aligned}$$

$$= O\left(n^{-\frac{3}{2\beta}} (\ln n)^{-\frac{1}{2}} \exp \sqrt{\frac{6x^2 b'}{a^2} \ln n} \right) \tag{A.12}$$

as $n \to \infty$, from the large x asymptotics of $\mathrm{Erf}(x)$ and here K, $\widetilde{K}$ are constants.

Next we claim that the dominating contribution of the integral in (A.11) comes from the integral $[n^{-3/2}, \varepsilon]$. To see this, it suffices to make a change of variable $r = ny$ and study

$$\begin{aligned} \mathcal{I}(n) &= \int_{n^{-3/2}}^{\varepsilon} \frac{\exp\left(-2ny \pm \sqrt{-\frac{4x^2 b'}{a^2} \ln(-iy)} \right) y^{\frac{1}{\beta}-1}}{\sqrt{-\ln(-iy)}} \, dy \\ &= \frac{1}{n^{\frac{1}{\beta}} \sqrt{\ln n}} \int_{n^{-1/2}}^{\varepsilon n} \frac{\exp\left[-2r \pm \sqrt{\frac{4x^2 b'}{a^2} \ln n \left(1 - \frac{\ln r - i\pi/2}{\ln n}\right)} \right]}{\sqrt{1 - \frac{\ln r - i\pi/2}{\ln n}}} \, r^{\frac{1}{\beta}-1} \, dr \end{aligned} \tag{A.13}$$

since for $x \neq 0$, $|\frac{\ln r - i\pi/2}{\ln n}| < 1$ over this interval and thus the inverse square root and the exponent in the numerator can be expanded. Then a term-by-term integration and extending the integration interval to $[0, \infty]$ produce a valid asymptotic series by the Dominated Convergence Theorem applied for any fixed n and by the fact that $\lim_{n\to\infty} \int_{n^{-1/2}}^{\epsilon n} e^{-2r} r^{\frac{1}{\beta}-1} (\ln r - i\pi/2)^j \, dr$ exists and is finite for any $j \geq 0$ and $\beta > 0$ (a very similar example can be found in Sec. 6.6 of [5]). At leading order, this yields

$$\mathcal{I}(n) \sim \frac{\exp\left(\pm \sqrt{\frac{4x^2 b'}{a^2} \ln n} \right)}{n^{\frac{1}{\beta}} \sqrt{\ln n}} \int_0^{\infty} e^{-2r} r^{\frac{1}{\beta}-1} \left[1 \mp \frac{\ln r - i\pi/2}{2\sqrt{\ln n}} \right] dr, \quad n \to \infty \tag{A.14}$$

so finally we obtain the asymptotic approximation

$$|C_{2n}| \sim \left| Re \left[\frac{\Gamma\left(\frac{1}{\beta}\right) e^{-\frac{x^2}{a} - i\frac{\pi}{2\beta}}}{(2n)^{\frac{1}{\beta}} \sqrt{\beta\pi \ln n}} \cosh \sqrt{\frac{4x^2 b'}{a^2} \ln n} \left(1 + i \frac{\pi \tanh \sqrt{\frac{4x^2 b' \ln n}{a^2}}}{4\sqrt{\ln n}} \right) \right] \right| \tag{A.15}$$

which dominates over (A.10) and (A.12). As a special case, when $x = 0$ and $\beta = \frac{1}{2k+1}$, $k = 0, 1, \ldots$, the leading order asymptotics of C_{2n} becomes proportional to $n^{-\frac{1}{\beta}} (\ln n)^{-\frac{3}{2}}$ because the term $\exp\left(-i\frac{\pi}{2\beta}\right)$ is pure imaginary and the tanh term in (A.15) vanishes.

For the shifted Chebyshev polynomials and $r(\xi) = \sqrt{\xi^3(1-\xi)}$, a similar formula is obtained following exactly the same procedure except that $\frac{1}{\beta}$ is replaced by $\frac{1}{\beta} + 1$.

ACKNOWLEDGMENTS

The authors thank Ken McLaughlin for helpful discussions. RMM, ZL, and AS were partially supported by a National Science Foundation Collaborations in Mathematical Geosciences (CMG) Award, NSF ATM-0327906. RMM was also partially supported by NSF DMS-030868. RC was partially supported by NSF DMS-0104329 and DMS-0509423. JCB was partially supported by NSF DMS-0354462. Computational work was supported by DMS-SCREMS 0422417. All wish to thank the suggestion made by the reviewers, especially regarding the connection between some of the singularities in the PDF and the extrema in the initial scalar field, and to explore the role of the scalar source in this model.

REFERENCES

1. M. Abramowitz and I. A. Stegun, *Handbook of Mathematical Functions with Formulas, Graphs, and Mathematical Tables, 9th Printing* Dover, New York, (1972).
2. R. A. Antonia and K. R. Sreenivasan, Log-normality of temperature dissipation in a turbulent boundary layer. *Phys. Fluids* **20**:1800–1804 (1977).
3. E. Balkovsky and A. Fouxon, Two complimentary descriptions of intermittency. *Phys. Rev. E.* **57**:R1231–R1234 (1998).
4. G. K. Batchelor, Small-scale variation of convected quantities like temperature in turbulent fluid, Part 1. General discussion and the case of small conductivity. *J. FLuid Mech.* **5**:113–133 (1959).
5. C. M. Bender and S. A. Orszag, *Advanced Mathematical Methods for Scientists and Engineers: Asymptotic Methods and Perturbation Theory* Springer-Verlag, New York, (2005)
6. A. Bourlioux, and A. J. Majda, Elementary models with probability distribution function intermittency for passive scalars with a mean gradient. *Phys. Fluids* **14**:881–897 (2002).
7. J. C. Bronski and R. M. McLaughlin, Passive scalar intermittency and the ground state of Schrödinger operators. *Phys. Fluids* **9**:181–190 (1997).
8. J. C. Bronski and R. M. McLaughlin, Rigorous estimates of the tails of the probability distribution function for the random linear shear model. *J. Stat. Phys* **98**(3/4):897–915 (2000).
9. B. Castaing, G. Gunaratne, F. Heslot, L. Kadanoff, A. Libchaber, S. Thomae, X-Z. Wu, S. Zaleski and G. Zanetti, Scaling of hard thermal turbulence in Rayleigh-Bénard convection. *J. Fluid Mech* **204**:1–30 (1989).
10. M. Chertkov, G. Falkovich and I. Kolokolov, Intermittent dissipation of a scalar in turbulence. *Phys. Rev. Lett* **80**:2121–2124 (1998).
11. R. M. Corless, D. J. Jeffrey and D. E. Knuth, A Sequence of Series for the Lambert Function. In *Proceedings of the 1997 International Symposium on Symbolic and Algebraic Computation, Maui, Hawaii* ACM Press, New York, (1997).
12. C. W. Gardiner, *Handbook of Stochastic Methods* Springer, New York, (2004).
13. M. Holzer and E. D. Siggia, Turbulent mixing of a passive scalar. *Phys. Fluids* **6**:1820–1837 (1994).

14. R. H. Kraichnan, Small-scale structure of a scalar field convected by turbulence. *Phys. Fluids* **11**:945–953 (1968).
15. A. J. Majda, Explicit inertial range renormalization theory in a model for turbulent diffusion, *J. Stat. Phys*. **73**:515 (1993).
16. A. J. Majda, The random uniform shear layer: an explicit example of turbulent diffusion with broad tail probability distributions. *Phys. Fluids A* **5**, 1963–1970 (1993).
17. A. J. Majda and P. Kramer, Simplified models for turbulent diffusion: Theory, numerical modelling, and physical phenomena. *Physics Reports* **314**:237–574 (1999).
18. J. C. Mason and D. C. Handscomb, *Chebyshev Polynomials* (Chapmen and Hall/CRC, Boca Raton, 2003).
19. R. M. McLaughlin and A. J. Majda, An explicit example with non-Gaussian probability distribution for nontrivial scalar mean and fluctuation. *Phys. Fluids* **8**:536–547 (1996).
20. R. T. Pierrehumbert, Lattice models of advection-diffusion. *Chaos* **10**:61–74 (2000).
21. S. C. Plasting and W. R. Young, A bound on scalar variance for the advection—diffusion equation. *J. Fluid Mech.* **552**:289–298 (2006).
22. W. Rudin, *Real and Complex Analysis* (McGraw-Hill, New York, 1966).
23. Z. S. She and S. A. Orszag, Physical model of intermittency in turbulence: Inertial range non-Gaussian statistics. *Phys. Rev. Lett.* **66**:1701–1704 (1991).
24. J.A. Shohat and J. D. Tamarkin, *The Problem of Moments* (American Mathematical Society, New York, 1943).
25. Y. G. Sinai and V. Yakhot, Limiting probability distributions of a passive scalar in a random velocity field. *Phys. Rev. Lett.* **63**:1962–1964 (1989).
26. L. C. Sparling and J. T. Bacmeister, Scale dependence of trace microstructure: Pdfs, intermittency and the dissipation scale. *Geophys. Res. Lett* **28**:2823–2826 (2001).
27. J. Thiffeault, C. R. Doering and J. D. Gibbon, A bound on mixing efficiency for the advection-diffusion equation. *J. Fluid Mech.* **521**:105–114 (2004).
28. S. T. Thoroddsen and C. W. Van Atta, Exponential tails and skewness of density-gradient probability density functions in stably stratified turbulence. *J. Fluid Mech* **244**:547–566 (1992).
29. E. Vanden-Eijnden. Non-Gaussian invariant measures for the Majda model of decaying turbulent transport. *Comm. Pure Appl. Math.* **54**(9):1146–1167 (2001).